Electronic Supplementary Material (ESI) for Journal of Materials Chemistry B.

– SUPPORTING INFORMATION –

Theranostic Inorganic-Organic Hybrid Nanoparticles with a Cocktail of Chemotherapeutic and Cytostatic Drugs

Mikhail Khorenko[1], Juliana Pfeifer[2], Joanna Napp[4,5], Anna Meschkov[2,3], Frauke Alves[4,5], Ute Schepers[2,3]*, and Claus Feldmann[1]**

Dr. M. Khorenko, Prof. Dr. C. Feldmann

[1] Institute of Inorganic Chemistry, Karlsruhe Institute of Technology (KIT), Engesserstraße 15, 76131 Karlsruhe, Germany. E-mail: claus.feldmann@kit.edu

J. Pfeifer, Dr. A. Meschkov, Prof. Dr. U Schepers

[2] Institute of Functional Interfaces, Karlsruhe Institute of Technology (KIT), Hermann-von-Helmholtz-Platz 1, 76344 Eggenstein-Leopoldshafen, Germany. E-mail: ute.schepers@kit.edu

[3] Institute of Organic Chemistry, Karlsruhe Institute of Technology (KIT), Fritz-Haber Weg 6, 76131 Karlsruhe, Germany

Priv.-Doz. Dr. J. Napp, Prof. Dr. F. Alves

[4] University Medical Center Goettingen (UMG), Institute for Diagnostic and Interventional Radiology, Robert Koch Str. 40, 37075 Goettingen, Germany

[5] Max Planck Institute for Multidisciplinary Sciences, Translational Molecular Imaging, City campus, Hermann-Rein-Strasse 3, 37075 Göttingen, Germany. E-mail: falves@gwdg.de

Content

1. Analytical Equipment

Scanning electron microscopy (SEM) was carried out with a Zeiss Supra 40 VP (Zeiss, Germany), equipped with a field emission gun (acceleration voltage 5 kV, working distance 3 mm). Samples were prepared by spraying a diluted aqueous suspension of the as-prepared IOH-NPs with a mist maker on a silica wafer that was left for drying overnight.

Energy-dispersive X-ray spectroscopy (EDXS) was performed with an Ametek EDAX device (Ametek, USA) mounted on the above described Zeiss SEM Supra 40 VP scanning electron microscope. For the analysis, the IOH-NPs were dried at 50°C and thereafter pressed to dense pellets in order to guarantee for a smooth surface and a quasi-infinite layer thickness. These pellets were fixed with conductive carbon pads on aluminium sample holders. An acceleration voltage of 30 kV was used for these measurements.

Dynamic light scattering (DLS) and *zeta potential* measurements were carried out on a Zetasizer Nano-ZS (Malvern, United Kingdom) with a 633 nm laser and backscattering geometry (173°). For DLS measurements, the aqueous IOH-NP suspensions were diluted 1:10 or 1:20 with demineralized water. The zeta potential of the as-prepared nanoparticles was also measured using these diluted aqueous suspensions.

Fourier-transform infrared (FT-IR) spectra were recorded on a Bruker Vertex 70 FT-IR spectrometer (Bruker, Germany) in the range from 4000 to 400 cm^{-1} with a resolution of 4 cm^{-1}. For this purpose, 1 mg of dried IOH-NPs was pestled with 300 mg of KBr and pressed to a pellet, which thereafter was measured in transmission.

Differential thermal analysis/thermogravimetry (DTA/TG) was performed with a STA409C device (Netzsch, Germany). The measurements were performed in air to guarantee for total combustion of the organic content. The IOH-NPs (20 mg in corundum crucibles), pre-dried at 100 °C for 5 h, were heated to 1200 °C with a rate of 5 K/min.

X-ray diffraction (XRD) measurements of the as-prepared IOH-NPs as well as of the residue after total organic combustion of these IOH-NPs (TG analysis) were performed with a Stadi MP diffractometer (STOE & Cie, Germany) using a Cu-$K_{\alpha 1}$ radiation source (λ = 154.05 pm) and a germanium-(111)-monochromator.

Elemental analysis (EA, C/H/N/S analysis) was performed via thermal combustion with an Elementar Vario Microcube device (Elementar, Germany) at a temperature of 1150 °C. The samples were pre-dried at 100°C for 5 h to remove the remaining solvent.

Photoluminescence (PL) measurements were performed with a Horiba Jobin Yvon Spex Fluorolog 3 (Horiba Jobin Yvon, France) equipped with a 450 W Xe-lamp and double-grating excitation and emission monochromators.

2. Material Characterization of IOH-NPs with Chemotherapeutic Cocktail

The cytostatic $Gd^{3+}{}_2[PMX]^{2-}{}_3$, $[Gd(OH)]^{2+}[EMP]^{2-}$, and $Gd^{3+}{}_2[(PMX)_{0.5}(EMP)_{0.5}]^{2-}{}_3$ IOH-NPs were characterized in regard of particle size, size distribution and colloidal stability, chemical composition and fluorescence labelling after modification with ICG or DUT (*see main paper Tables 1,2, Figures 2,3*; Figures S1-S7).

Particle size and colloidal properties were characterized based on scanning electron microscopy (SEM), dynamic light scattering (DLS), and zeta-potential analysis (*see main paper Table 1, Figure 2*; Figures S1-S5). Thus, the IOH-NPs exhibit particle diameters of 40 to 60 nm according to SEM and hydrodynamic diameters of 60 to 100 nm according to DLS. Zeta-potential measurements shown negative charging of –15 to –35 mV. According to x-ray diffraction (XRD), the IOH-NPs are non-crystalline (Figure S4). Fourier-transform infrared (FT-IR) spectroscopy evidences the presence of the respective cytostatic anion (*see main paper Figure 2*; Figures S1-S5). The characteristic vibrations of the cytostatic anions are observed and well in agreement with the starting materials as references (PMX: *ν*(C–H): 3000-2800, *ν*(C=O): 1800-1650, *ν*(C=C): 1680-1610, *ν*(C–N): 1340-1260, *ν*(C–O): 1085-1050, fingerprint area: 1000-400 cm^{-1}; EMP: *ν*(C–H): 3000-2800, *ν*(C=O): 1800-1650, *ν*(C=C): 1680-1610, *ν*(PO_4): 1250-1000, *ν*(C–N): 1250-1020, *ν*(C–O): 1085-1050, fingerprint area: 1000-400 cm^{-1}).

Total organics combustion via thermogravimetry (TG) and elemental analysis (EA) confirm the chemical composition of the IOH-NPs (*see main paper Table 2*; Figures S1-S5). Finally, the thermal remnants of the TG analyses were analysed by XRD, resulting in Gd_2O_3, $GdPO_4$, and Gd_3PO_7 as residual phases (Figure S5). After correcting the experimental data for a release of 5.0 wt-% of adsorbed H_2O (Table S1, Figure S1), the thermal decomposition of $[Gd]^{3+}{}_2[PMX]^{2-}{}_3$ can be ascribed to the following reaction: $2\ Gd^{3+}{}_2[C_{20}H_{19}N_5O_6]^{2-}{}_3 + 133.5\ O_2 \rightarrow 2\ Gd_2O_3 + 120\ CO_2 + 15\ N_2 + 57\ H_2O$.

For $[Gd(OH)]^{2+}[EMP]^{2-}$ the experimental data were also corrected for 5.0 wt-% of adsorbed water (Table S1, Figure S2) and relate to a thermal decomposition according to: 2 $[Gd(OH)]^{2+}[C_{23}H_{30}Cl_2NO_6P]^{2-}$ + 58.5 O_2 → 2 $GdPO_4$ + 46 CO_2 + N_2 + 4 HCl + 29 H_2O.

For $Gd^{3+}{}_2[(PMX)_{0.5}(EMP)_{0.5}]^{2-}{}_3$, after correcting the experimental TG values by 5.0 wt-% of adsorbed water (Table S1, Figure S3), the thermal decomposition is in accordance with the reaction: 2 $Gd^{3+}{}_2[(C_{20}H_{19}N_5O_6)_{0.5}(C_{23}H_{30}Cl_2NO_6P)_{0.5}]^{2-}{}_3$ + 153 O_2 → $GdPO_4$ + Gd_3PO_7 + 129 CO_2 + 9 N_2 + 6 HCl + 0.25 P_4O_{10} + 70.5 H_2O.

Table S1. Data of the thermogravimetric analysis with correction of the experimental data for the amount of absorbed water.

	Weight loss / %	**Amount of adsorbed water / %**	**Corrected weight loss / %**
$Gd^{3+}{}_2[PMX]^{2-}{}_3$	73.2	5.0	77.1
$Gd^{3+}{}_2[(PMX)_{0.5}(EMP)_{0.5}]^{2-}{}_3$	67.6	5.0	71.2
$[Gd(OH)]^{2+}[EMP]^{2-}$	61.3	5.0	64.5

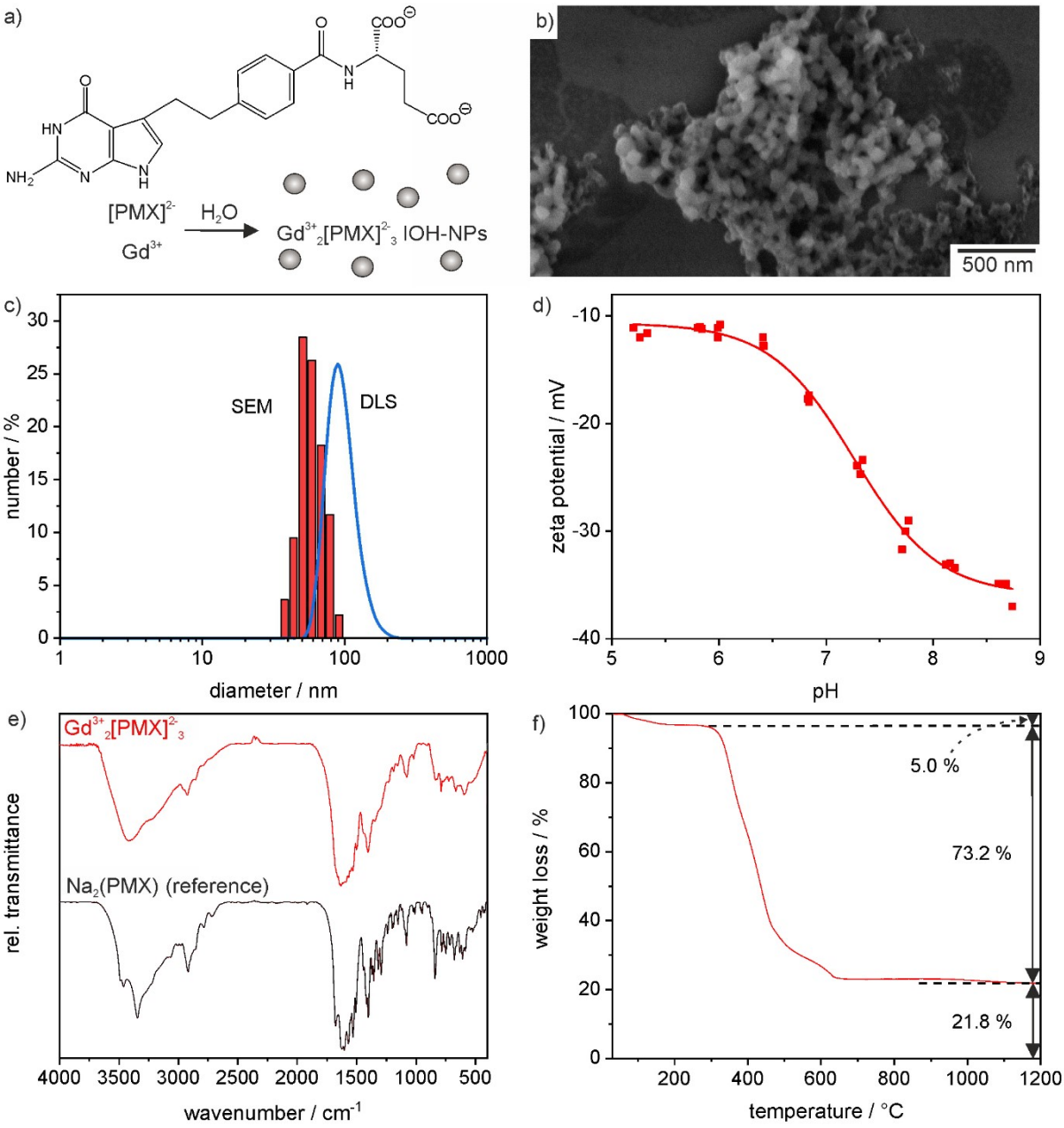

Figure S1. Particle characterization and chemical composition of $Gd^{3+}_2[PMX]^{2-}_3$ IOH-NPs: a) Scheme of synthesis with structure of anion, b) Particle size and shape according to SEM, c) Particle size distribution according to DLS and SEM, d) Zeta potential of aqueous suspension, e) FT-IR spectrum with pure PMX as a reference, f) TG analysis.

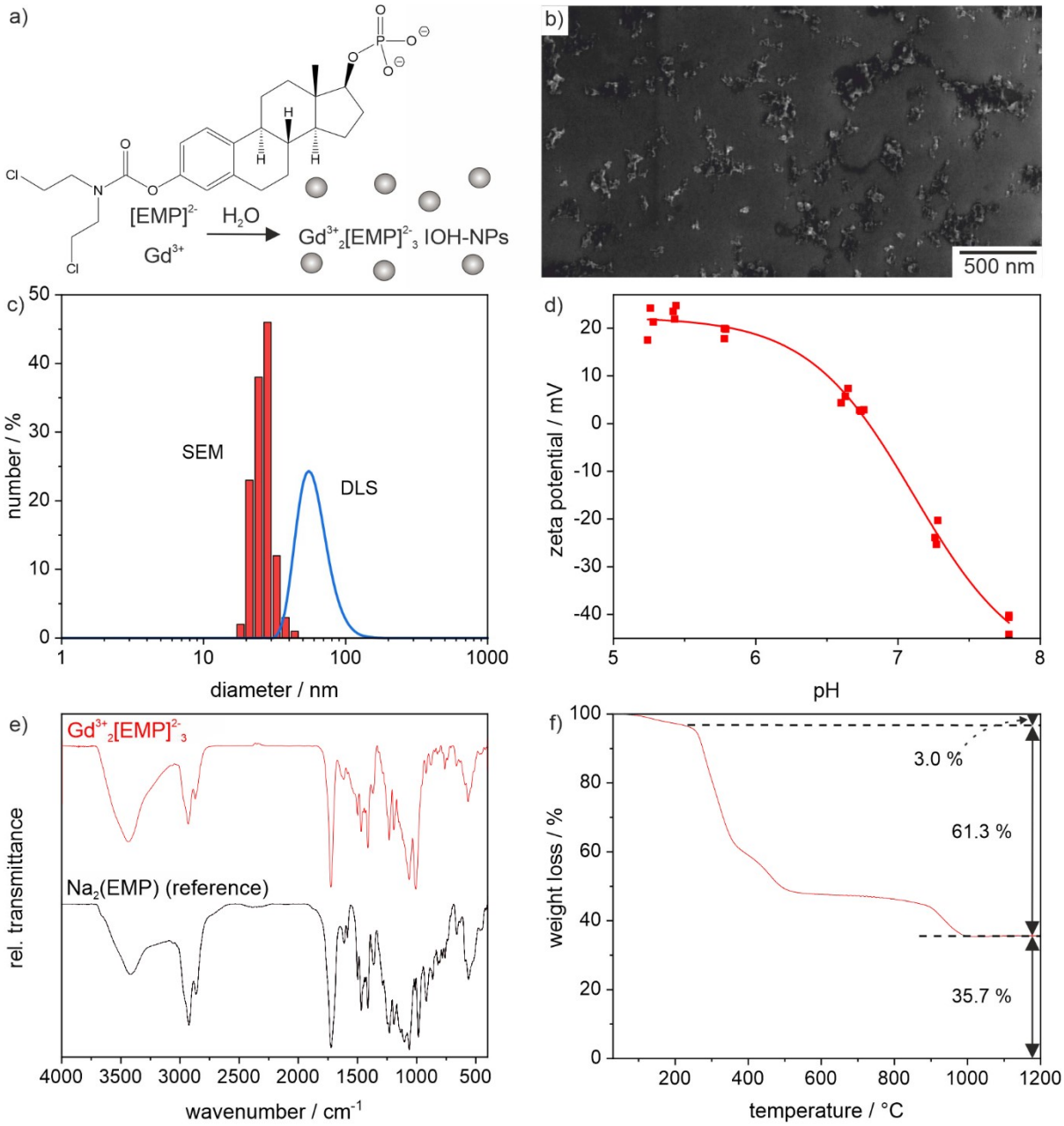

Figure S2. Particle characterization and chemical composition of $Gd^{3+}_2[EMP]^{2-}_3$ IOH-NPs: a) Scheme of synthesis with structure of anion, b) Particle size and shape according to SEM, c) Particle size distribution according to DLS and SEM, d) Zeta potential of aqueous suspension, e) FT-IR spectrum with pure EMP as a reference, f) TG analysis.

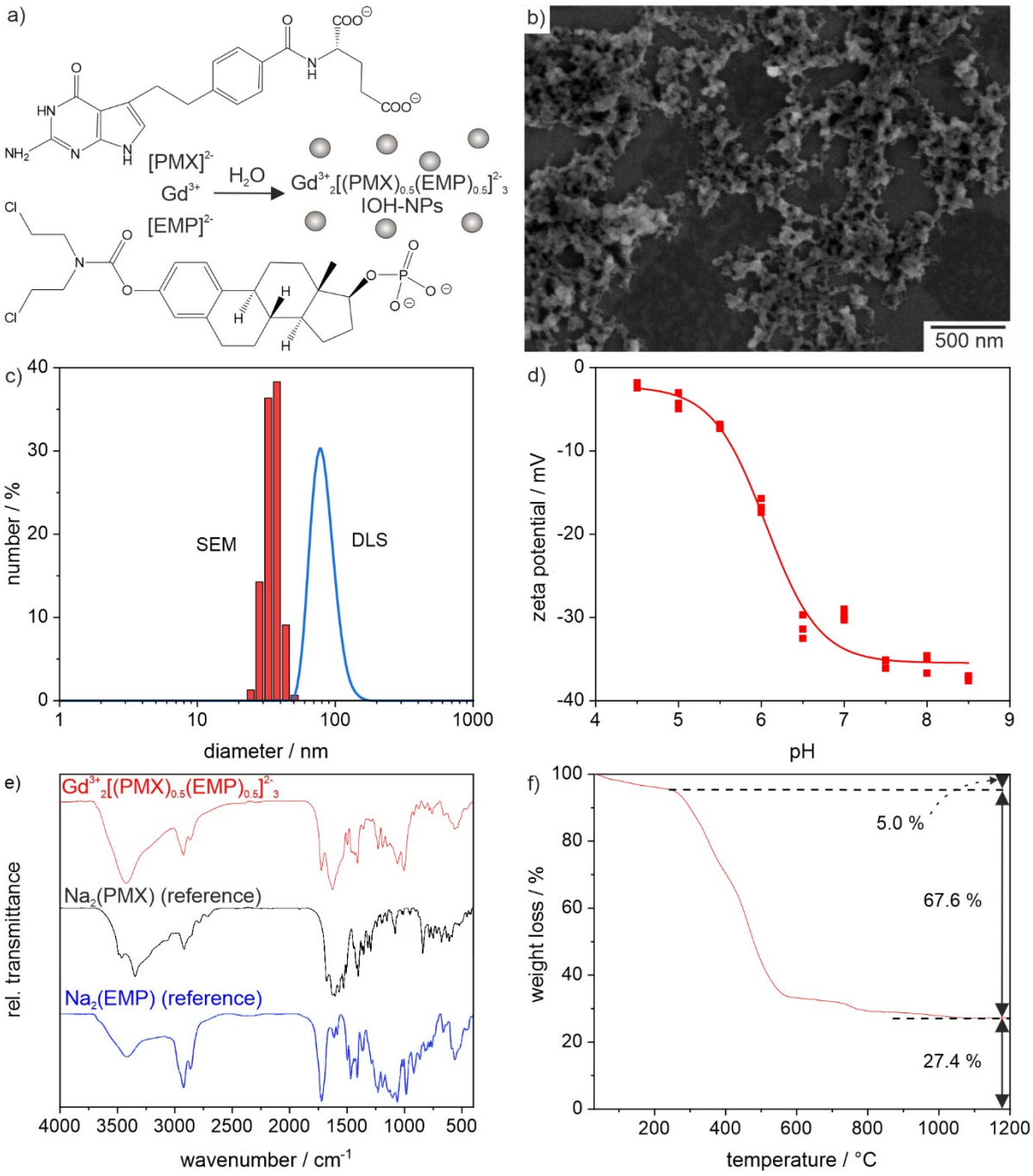

Figure S3. Particle characterization and chemical composition of $Gd^{3+}{}_2[(PMX)_{0.5}(EMP)_{0.5}]^{2-}{}_3$ IOH-NPs: a) Scheme of synthesis with structure of anion, b) Particle size and shape according to SEM, c) Particle size distribution according to DLS and SEM, d) Zeta potential of aqueous suspension, e) FT-IR spectrum with pure PMX and EMP as references, f) TG analysis.

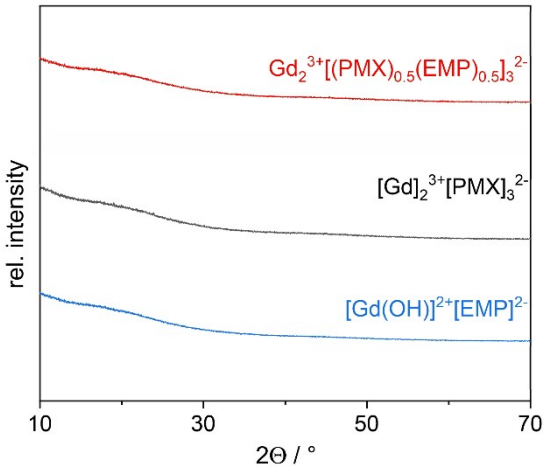

Figure S4. XRD analysis of the as-prepared $Gd^{3+}_2[PMX]^{2-}_3$, $[Gd(OH)]^{2+}[EMP]^{2-}$, and $Gd^{3+}_2[(PMX)_{0.5}(EMP)_{0.5}]^{2-}_3$ IOH-NPs.

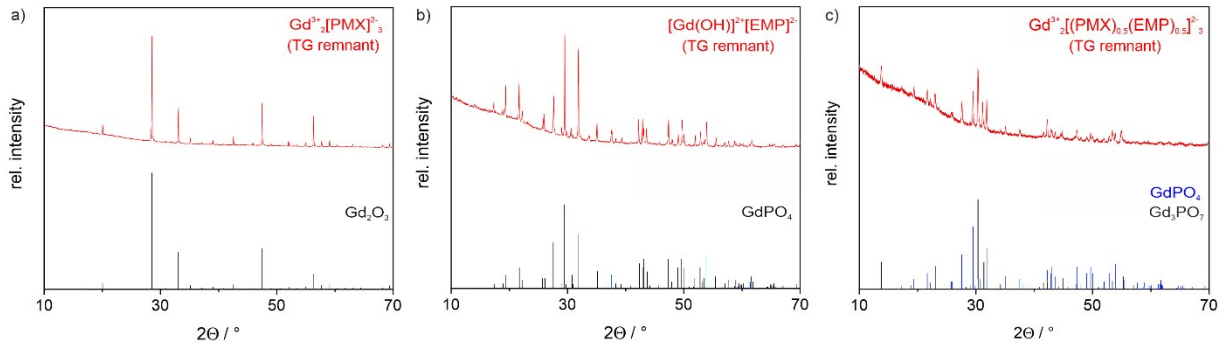

Figure S5. XRD analysis of the thermal remnant of the $Gd^{3+}_2[PMX]^{2-}_3$, $[Gd(OH)]^{2+}[EMP]^{2-}$, and $Gd^{3+}_2[(PMX)_{0.5}(EMP)_{0.5}]^{2-}_3$ IOH-NPs after TG analysis with heating to 1200 °C (Gd_2O_3/ICDD-No. 00-043-1014, $GdPO_4$/ICDD-No. 00-032-0386, Gd_3PO_7/ICDD-No. 00-034-1066 as references)

To enable the IOH-NPs with chemotherapeutic cocktail for fluorescence-based monitoring, they were labelled with indocyanine green (ICG) or Dyomics DY-647-dUTP (DUT) as a fluorescent dyes (Figures S6).

ICG is clinically approved and known for deep-red emission, which, however, is weak for freely dissolved ICG.[S1] Due to the great number of ICG anions in a single IOH-NP, however, the deep-red emission is here sufficient for fluorescence detection. On the other hand, the ICG load is nevertheless low (about 5-6 mol-%) in comparison to the drug load, so that the drug load per nanoparticle is reduced only slightly. This is expressed by the chemical formula $Gd^{3+}_2[(PMX)_{0.96}(ICG)_{0.08})]^{2-}_3$, $[Gd(OH)]^{2+}[(EMP)_{0.94}(ICG)_{0.12})]^{2-}$, and $Gd^{3+}_2[(PMX)_{0.50}(EMP)_{0.47}(ICG)_{0.06}]^{2-}_3$. Successful ICG incorporation is visible even with the naked eye due to the greenish colour of the IOH-NPs and quantified by optical spectroscopy

(Figure S6a). Fluorescence spectra of the ICG-modified IOH-NPs confirm the characteristic excitation at 600-800 nm (peaking at 780 nm) and the deep-red emission at 750-850 nm (peaking at 810 nm).

DUT shows intense deep-red emission and is required only with very small amounts (1 mol-%), resulting in the chemical formula $Gd^{3+}{}_2[(PMX)_{0.99}(DUT)_{0.01})]^{2-}{}_3$, $[Gd(OH)]^{2+}[(EMP)_{0.99}(DUT)_{0.01})]^{2-}$ and $Gd^{3+}{}_2[(PMX)_{0.50}(EMP)_{0.49}(DUT)_{0.02}]^{2-}{}_3$. Successful DUT incorporation is also visible with the naked eye due to the bluish colour of the IOH-NPs and quantified by optical spectroscopy (Figure S6b). Fluorescence spectra of the DUT-modified IOH-NPs confirm the characteristic excitation at 500-700 nm (peaking at 655 nm) and the deep-red emission at 630-780 nm (peaking at 675 nm).

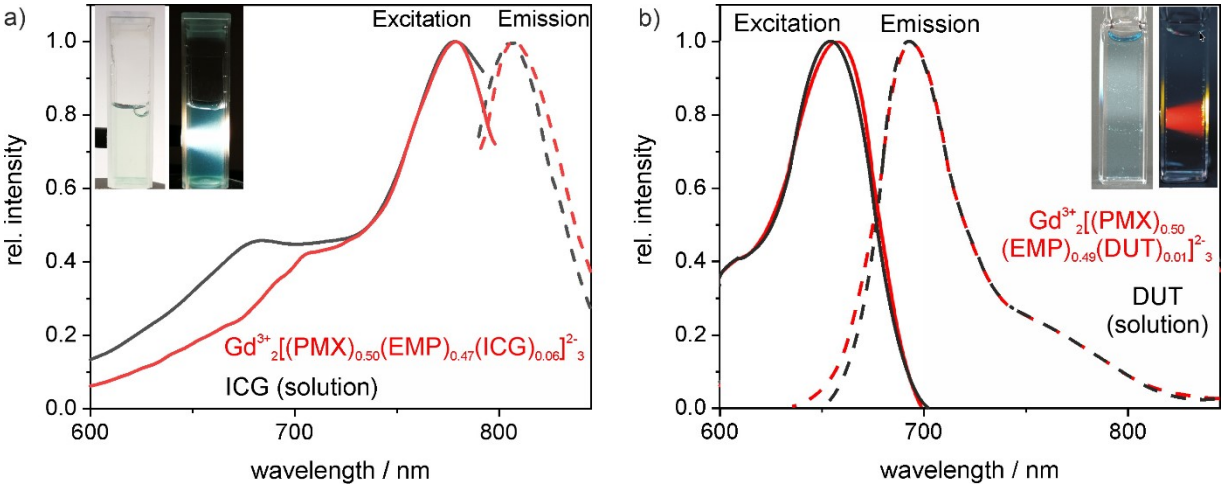

Figure S6. Excitation and emission spectra of the dual-function IOH-NPs: a) ICG-modified $Gd^{3+}{}_2[(PMX)_{0.50}(EMP)_{0.47}(ICG)_{0.06}]^{2-}{}_3$, b) DUT-modified $Gd^{3+}{}_2[(PMX)_{0.50}(EMP)_{0.49}$-$(DUT)_{0.01}]^{2-}{}_3$ (with freely dissolved ICG and DUT as references).

3. Material Characterization of IOH-NPs with Cytotoxic and Phototoxic Agents

Similar to the cytostatic IOH-NPs, SEM and DLS show particle size, colloidal properties, and zeta-potential of the $[Gd(OH)]^{2+}[(PMX)_{0.74}(AlPCS_4)_{0.13}]^{2-}$ and $[Gd(OH)]^{2+}[(PMX)_{0.70}(TPPS_4)_{0.15}]^{2-}$ IOH-NPs (*see main paper Table 1, Figure 2*; Figures S7,S8). Again, the IOH-NPs exhibit particle diameters of 40 to 60 nm (SEM) and hydrodynamic diameters of 60 to 100 nm (DLS) and negative charging of –15 to –35 mV. FT-IR spectra evidence the presence of PMX, $AlPCS_4$ or $TPPS_4$ (*see main paper Figure 2*; Figures S7,S8). The characteristic vibrations of the cytostatic and the photosensitizing anions are observed and well in agreement with the starting materials as references (PMX: ν(C–H):

3000-2800, *ν*(C=O): 1800-1650, *ν*(C=C): 1680-1610, *ν*(C–N): 1340-1260, *ν*(C–O): 1085-1050, fingerprint area: 1000-400 cm^{-1}; $AlPCS_4$: *ν*(N–H): 3500-3330, *ν*(C–H): 3000-2750, *ν*(C=C): 1680-1610, *ν*(C=N): 1660-1480, *ν*(SO_3): 1600-1300, 1250-950, *ν*(C–N): 1340-1260 cm^{-1}; $TPPS_4$: *ν*(N–H): 3500-3330, *ν*(C–H): 3000-2750, *ν*(C=C): 1680-1610, *ν*(C=N): 1660-1480, *ν*(SO_3): 1600-1300, 1250-950, *ν*(C-N): 1340-1260 cm^{-1}).

Total organics combustion via thermogravimetry (TG) and elemental analysis (EA) confirm the chemical composition of the IOH-NPs (*see main paper Table 2*; Figures S7,S8). The thermal remnants of the TG analyses were analysed by XRD, resulting in Gd_2O_3 and $Gd_4Al_2O_9$ (Figure S9). After correcting the experimental data for a release of 3.0 wt-% of adsorbed H_2O (Table S2, Figure S7), the thermal decomposition of $[Gd(OH)]^{2+}[(PMX)_{0.74}(AlPCS_4)_{0.13}]^{2-}$ can be ascribed to the following reaction: 2 $[Gd(OH)]^{2+}[(C_{20}H_{19}N_5O_6)_{0.74}(C_{32}H_{12}AlClN_8O_{12}S_4)_{0.13}]^{2-}$ + 41.9 O_2 → 0.74 Gd_2O_3 + 0.13 $Gd_4Al_2O_9$ + 37.92 CO_2 + 16.49 H_2O + 9.48 N_2 + 0.26 HCl + 1.04 SO_2.

For $[Gd(OH)]^{2+}[(PMX)_{0.70}(TPPS_4)_{0.15}]^{2-}$, the thermal decomposition can be ascribed to the following reaction after correcting the experimental data for 3.0 wt-% of adsorbed H_2O (Table S2, Figure S8): 2 $Gd^{3+}{}_2[(C_{20}H_{19}N_5O_6)_{0.5}(C_{23}H_{30}Cl_2NO_6P)_{0.5}]^{2-}{}_3$ + 153 O_2 → $GdPO_4$ + Gd_3PO_7 + 129 CO_2 + 9 N_2 + 6 HCl + 0.25 P_4O_{10} + 70.5 H_2O.

Table S2. Data of the thermogravimetric analysis with correction of the experimental data for the amount of absorbed water.

	Weight loss / %	**Amount of adsorbed water / %**	**Corrected weight loss / %**
$[Gd(OH)]^{2+}[(PMX)_{0.74}(AlPCS_4)_{0.13}]^{2-}$	67.4	3.0	69.5
$[Gd(OH)]^{2+}[(PMX)_{0.70}(TPPS_4)_{0.15}]^{2-}$	70.5	3.0	72.7

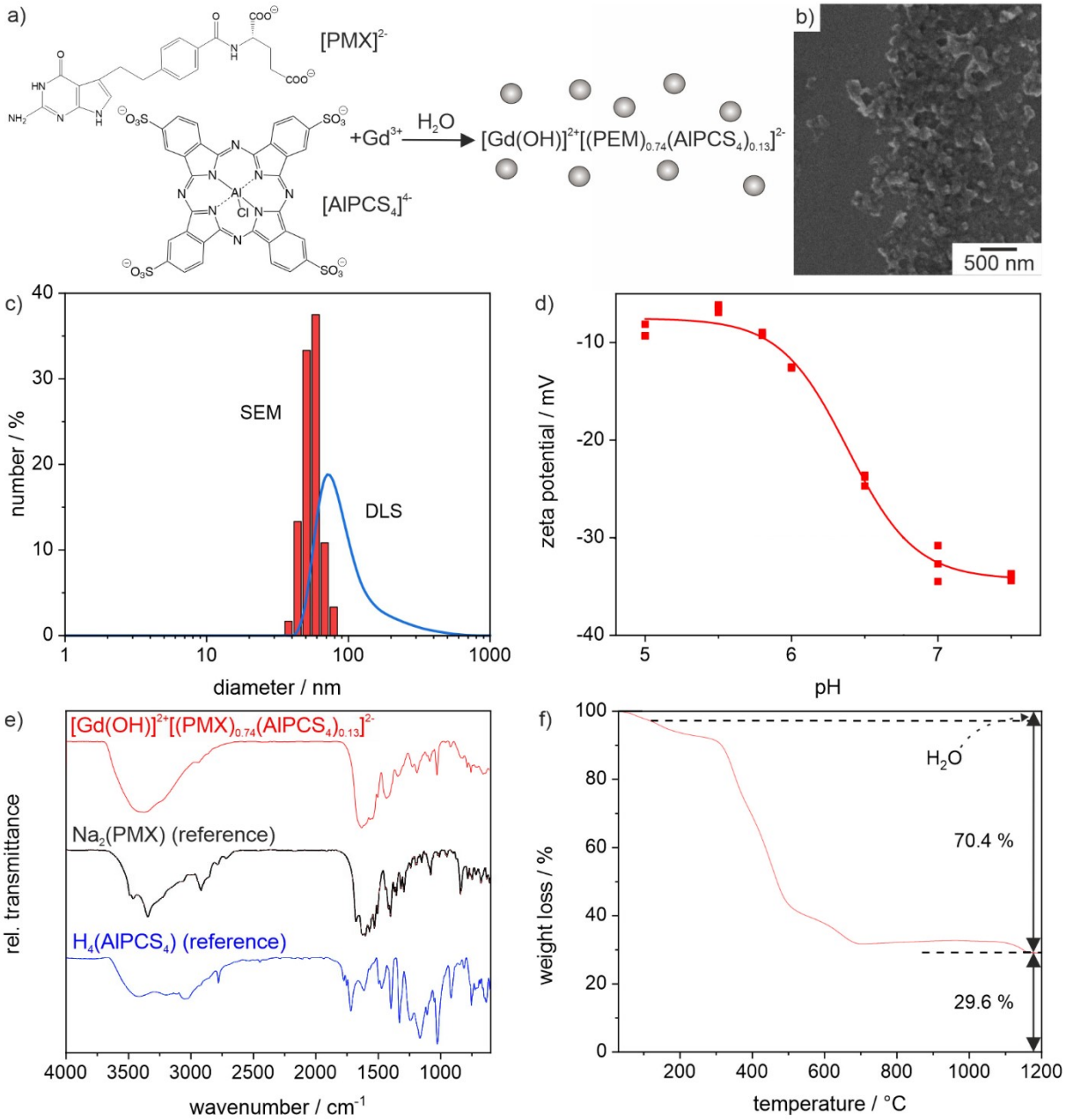

Figure S7. Particle characterization and chemical composition of $[Gd(OH)]^{2+}[(PMX)_{0.74}(AlPCS_4)_{0.13}]^{2-}$ IOH-NPs: a) Scheme of synthesis with structure of anion, b) Particle size and shape according to SEM, c) Particle size distribution according to DLS and SEM, d) Zeta potential of aqueous suspension, e) FT-IR spectrum with pure PMX and $AlPCS_4$ as references, f) TG analysis.

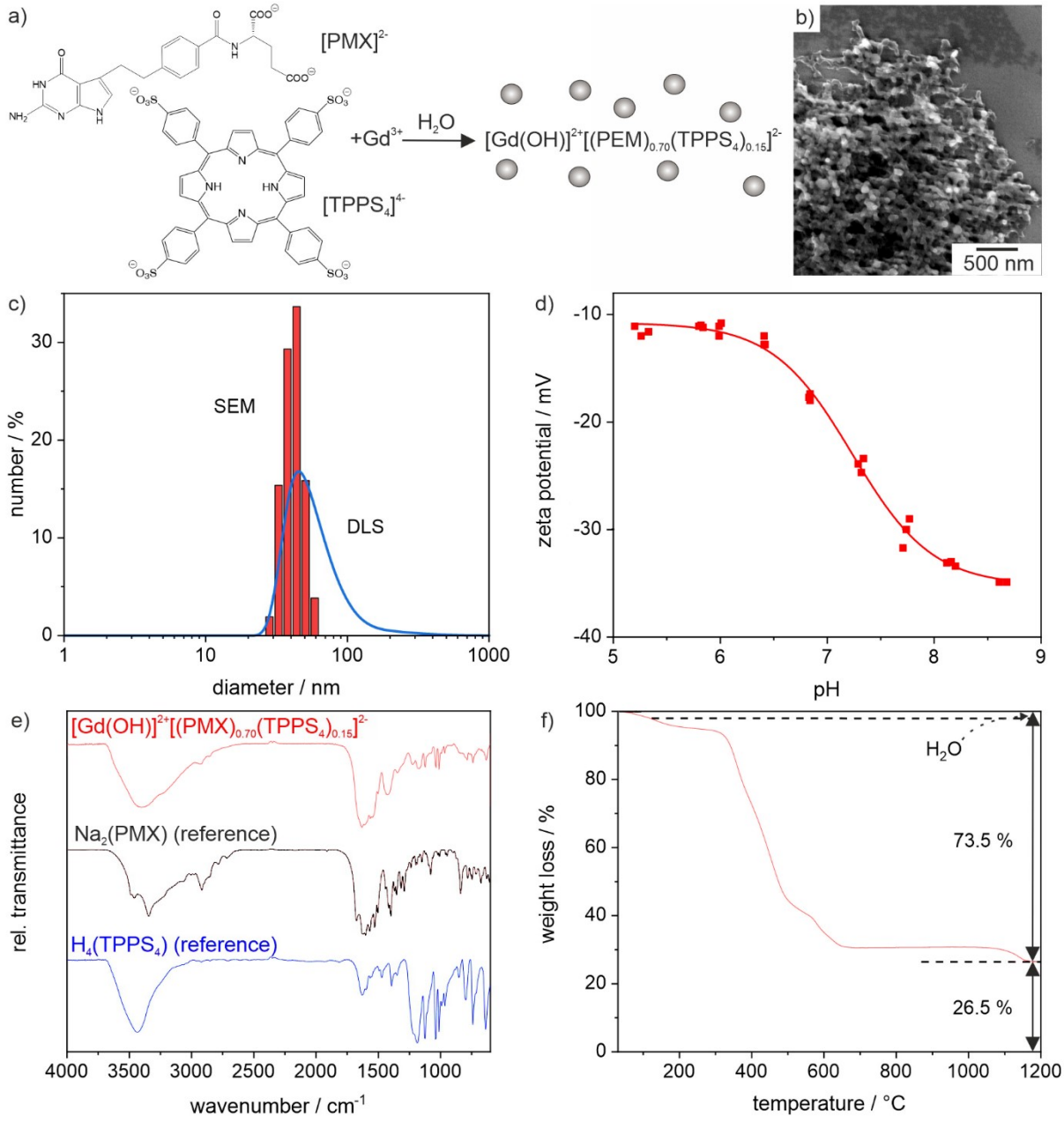

Figure S8. Particle characterization and chemical composition of $[Gd(OH)]^{2+}[(PMX)_{0.70}(TPPS_4)_{0.15}]^{2-}$ IOH-NPs: a) Scheme of synthesis with structure of anion, b) Particle size and shape according to SEM, c) Particle size distribution according to DLS and SEM, d) Zeta potential of aqueous suspension, e) FT-IR spectrum with pure PMX and $TPPS_4$ as references, f) TG analysis.

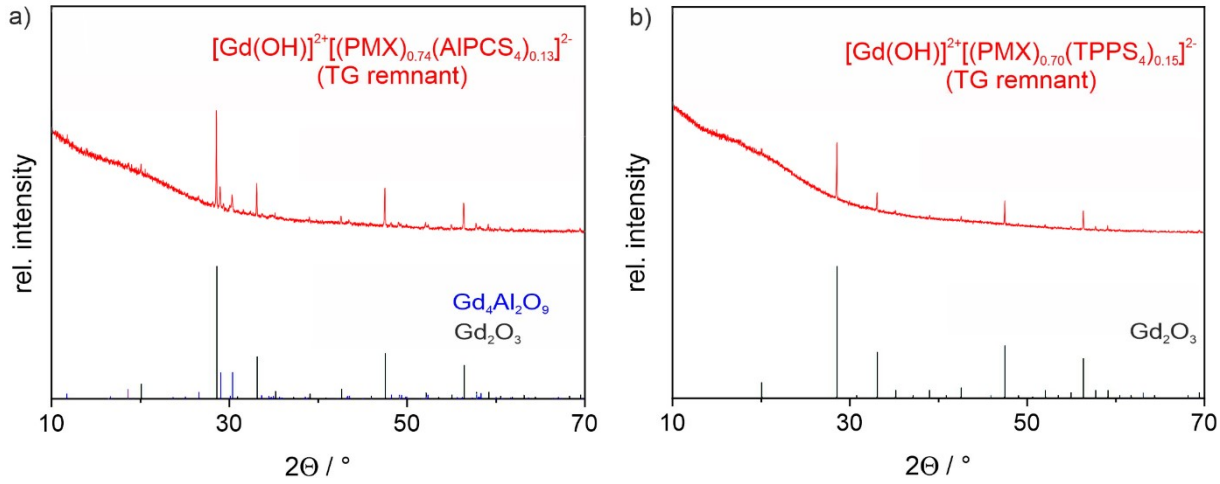

Figure S9. XRD analysis of the thermal remnant of the $[Gd(OH)]^{2+}[(PMX)_{0.74}(AlPCS_4)_{0.13}]^{2-}$ and $[Gd(OH)]^{2+}[(PMX)_{0.70}(TPPS_4)_{0.15}]^{2-}$ IOH-NPs after TG analysis with heating to 1200 °C (Gd_2O_3/ICDD-No. 00-086-2477, $Gd_4Al_2O_9$/ICDD-No. 00-046-0396 as references).

In contrast to the dual-function cytostatic IOH-NPs, the phototoxic $[Gd(OH)]^{2+}[(PMX)_{0.74}(AlPCS_4)_{0.13}]^{2-}$ and $[Gd(OH)]^{2+}[(PMX)_{0.70}(TPPS_4)_{0.15}]^{2-}$ IOH-NPs show fluorescence themselves. The characteristic absorption of $AlPCS_4$ and $TPPS_4$ is visible with the naked eye and can be quantified by PL spectra. Thus, $[Gd(OH)]^{2+}[(PMX)_{0.74}(AlPCS_4)_{0.13}]^{2-}$ shows strong absorption at 550-720 nm and deep-red emission at 650-770 nm (peaking at 686 nm) (Figure S10a). $[Gd(OH)]^{2+}[(PMX)_{0.70}(TPPS_4)_{0.15}]^{2-}$ absorbs at 380-600 nm and emits at 540-700 nm (peaking at 585 nm) (Figure S10b).

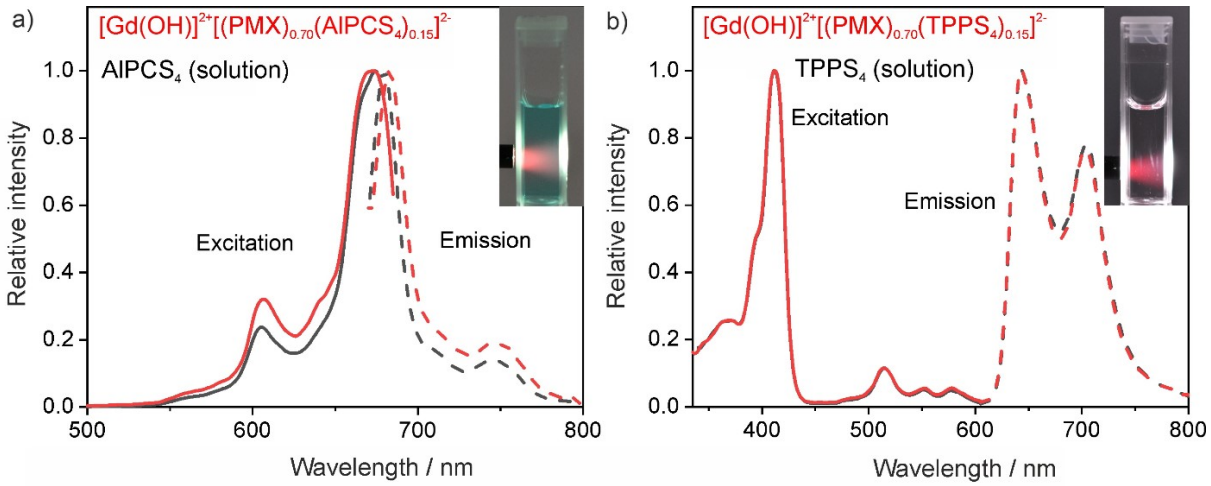

Figure S10. PL spectra of the $[Gd(OH)]^{2+}[(PMX)_{0.74}(AlPCS_4)_{0.13}]^{2-}$ and $[Gd(OH)]^{2+}[(PMX)_{0.70}(TPPS_4)_{0.15}]^{2-}$ IOH-NPs (freely dissolved $AlPCS_4$ and $TPPS_4$ as references).

4. *In vitro* Studies for IOH-NPs with Chemotherapeutic Cocktail

Cell culture. The adherent human pancreatic cancer cell line AsPC-1 was purchased from ATCC (Rockville, USA). The adherent murine breast cancer cell line pH8N8 was maintained and cultured as described before.[S2] Cells were cultivated at 37 °C in a humidified atmosphere of 5% CO_2. AsPC1 cells were grown in RPMI-1640 media (Life Technologies, Germany) and pH8N8 cells were grown in Dulbecco's Modified Eagle's Medium (DMEM, Life Technologies, Germany), both supplemented with 10% fetal bovine serum (FBS Gold, PAA Laboratories Gold).

Confocal fluorescence microscopy. To study IOH-NP uptake, pH8N8 or AsPC1cells were plated in a concentration of 50.000 cells per well on poly-L-lysine-coated glass-cover slips and allowed to attach for two days. Afterwards, the cell-culture medium was replaced by a fresh medium supplemented with 50 µL/mL of $Gd_2^{3+}[(PMX)_{0.50}(EMP)_{0.49}(DUT)_{0.01}]_3^{2-}$ IOH-NPs. After the defined incubation times (30 min, 2, 5, 24, 48 h) cells were washed twice with phosphate-buffered saline (PBS), fixed with 4% paraformaldehyde (PFA) for 10 min at room temperature (RT), counterstained with DAPI (1:1000 in PBS; Thermo Fisher Scientific, Germany) and mounted with a mounting medium (Immu-Mount, Thermo Scientific, Germany). The ICG-derived fluorescence was recorded using a high sensitivity ORCA-AG digital camera (Hamamatsu, Japan) and the 708/75 nm bandpass filter for the excitation and 809/81 nm bandpass filter for the emission. DAPI was excited at 365/25 nm. The emission (blue) was collected at 445/50 nm. The DUT-derived fluorescence was visualized using an SP5 confocal microscope (Leica, Germany). DAPI was excited with a 405 nm laser, and the emission was collected at 415-500 nm. DUT was excited using a 633 nm laser, and the emission was collected at 645-780 nm. Image generation and processing were performed with the AxioVision Rel.4.6 software (Zeiss, Germany) and FIJI[S3] (National Institutes of Health, USA) (Figure S11; s*ee main paper: Figure 3*).

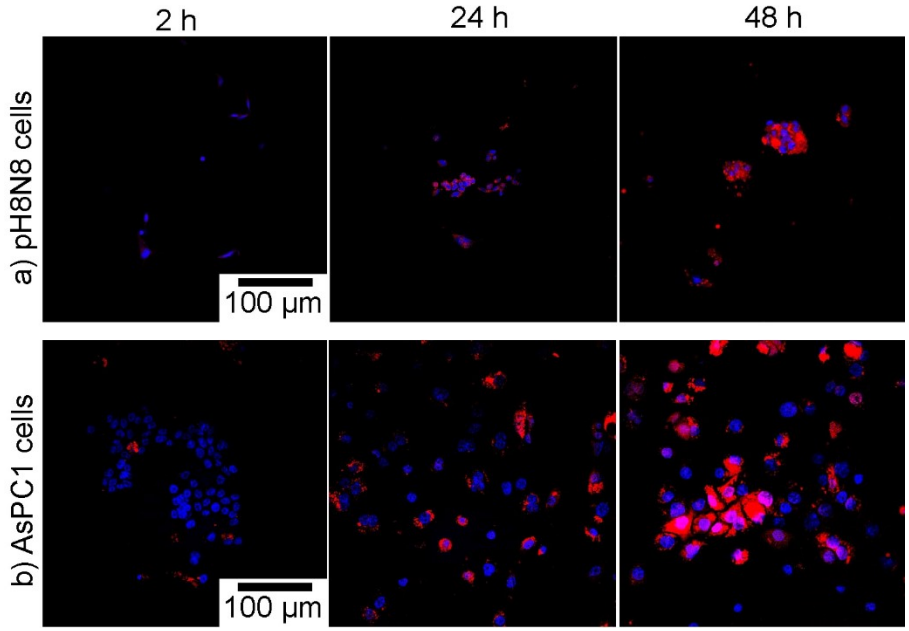

Figure S11. Time-dependent uptake of DUT-labelled $Gd_2^{3+}[(PMX)_{0.50}(EMP)_{0.49}(DUT)_{0.01}]_3^{2-}$ IOH-NPs by (a) pH8N8 cells and (b) AsPC1 cells (5×10^5 cells per well) incubated over 2-48 h with 50 µL/mL of IOH-NPs. DAPI was excited with 405 nm laser and the emission collected at 415-500 nm. DUT was excited using a 633 nm laser and the emission collected at 645-780 nm (identical scale bar for all images, see main paper: *Figure 3* for high-resolution images).

Efficacy analysis. To analyse the efficacy of IOH-NPs with chemotherapeutic cocktail, MTT-based viability assays were performed (Figures S12,S13; *see main paper: Figure 4*). AsPC1 and pH8N8 cells were plated in a 96-well plate in a concentration of 10.000 cells per well in the corresponding cell-culture medium and allowed to attach overnight. On the next day, the cell-culture medium was replaced by 200 µL of fresh medium (green pillars) or medium supplemented with increasing amounts (1, 5, 10, 50 µL) of $Gd^{3+}{}_2[PMX]^{2-}{}_3$, $[Gd(OH)]^{2+}[EMP]^{2-}$ and $Gd^{3+}{}_2[(PMX)_{0.5}(EMP)_{0.5}]^{2-}{}_3$ IOH-NPs (blue pillars) as well as the corresponding freely dissolved drugs (i.e. $Na_2(PMX)\times7H_2O$, $Na_2(EMP)$, $Na_2(PMX)\times7H_2O/Na_2(EMP)$ 1:1 mixture; grey pillars: Figures S12,S13; *see main paper: Figure 4*). The metabolic activity was assessed either directly after adding the IOH-NPs or dissolved drugs (0 h) as well as after 24 and 72 h of treatment using CellTiter 96® AQueous One Solution Cell Proliferation Assay (Promega). The absorbance of the metabolised substrate was measured at 490 nm. The experiment was performed in triplicate. Additionally, the absorbance of each substance diluted in the medium (IOH-NPs or dissolved drugs) was measured in cell-free conditions (black pillars: Figures S12,S13; *see main paper: Figure 4*).

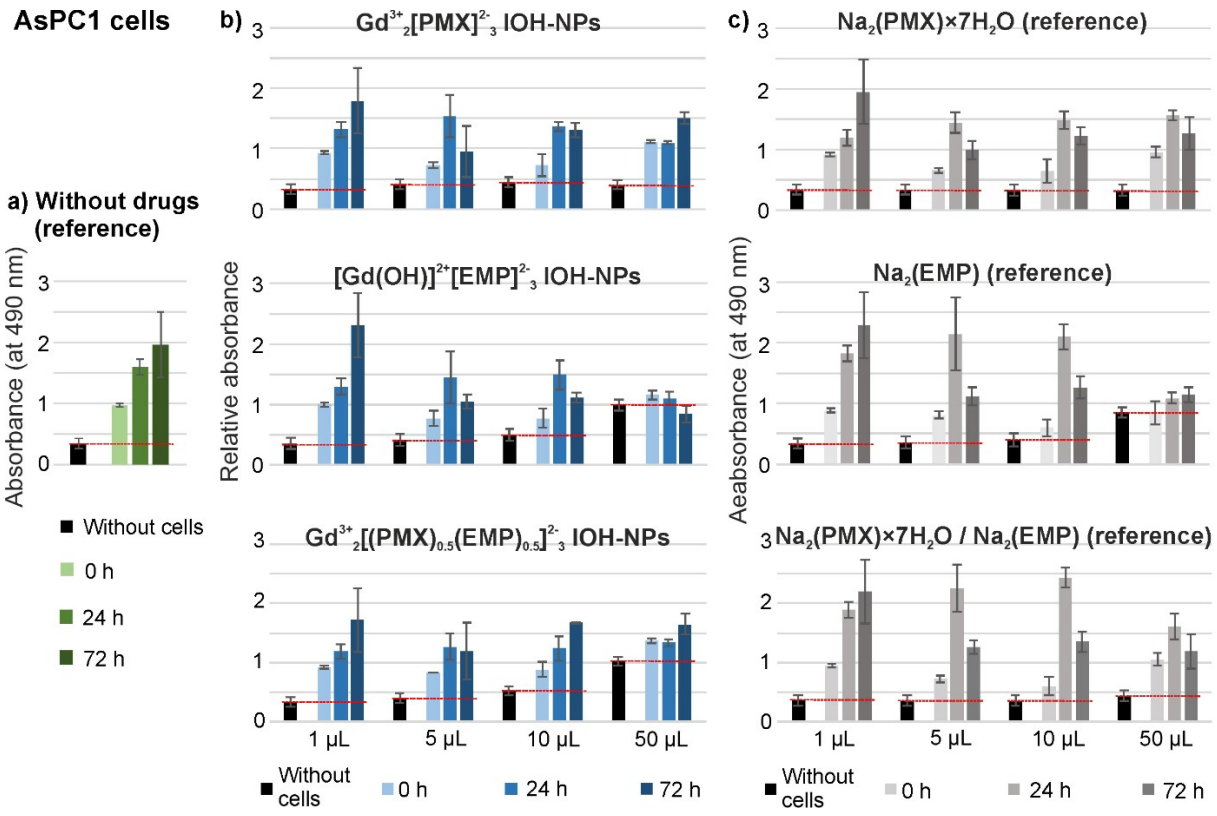

Figure S12. *In vitro* studies of IOH-NPs with single drug and chemotherapeutic cocktail on AsPC1 cells. MTT-based viability test after 0 to 72 h of treatment with (a) untreated cells, (b) treated with the indicated IOH-NP concentration (1-50 µL/200 µL), and (c) treated with the freely dissolved drugs. The concentrations of the freely dissolved drugs were according to their dose in the IOH-NPs. Dotted red lines indicate the self-absorption of medium, cells, and/or drugs. Error bars correspond to standard error of $n = 4$.

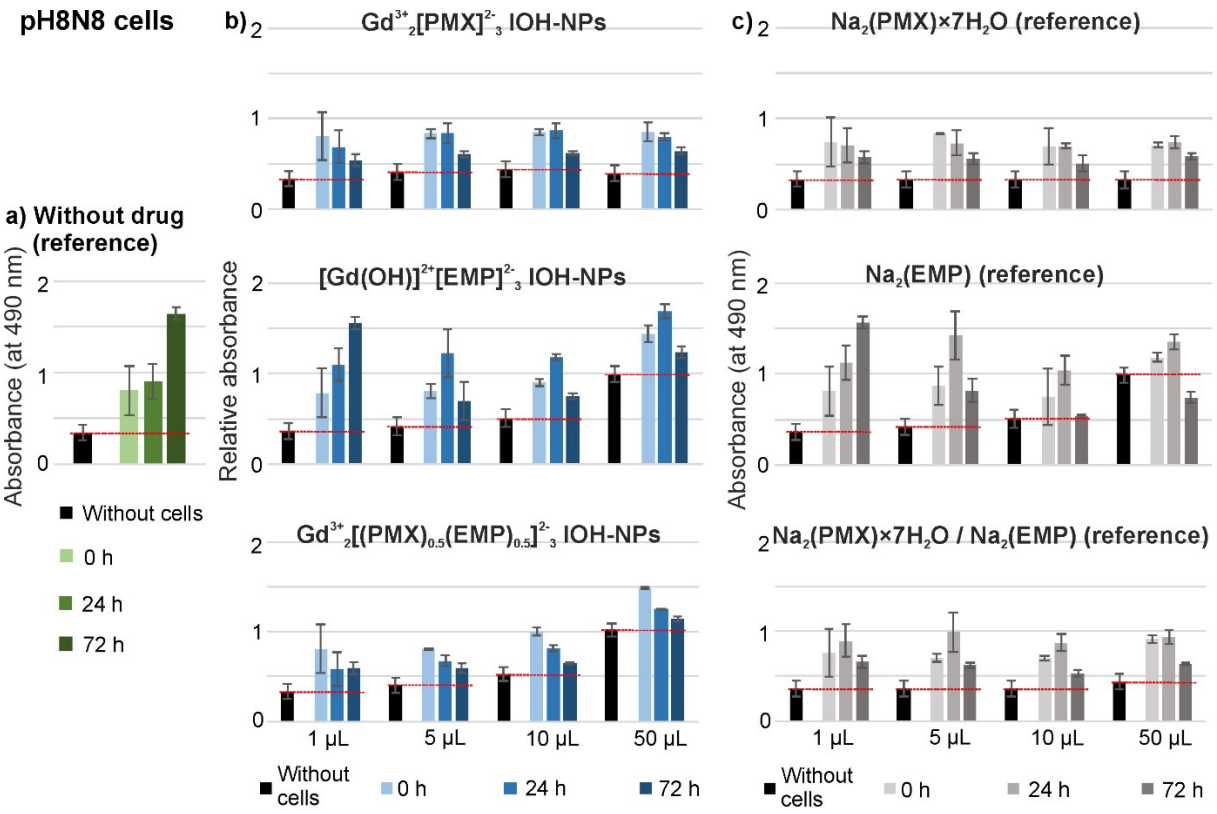

Figure S13. *In vitro* studies of IOH-NPs with single drug and chemotherapeutic cocktail on pH8N8 cells. MTT-based viability test after 0 to 72 h of treatment with (a) untreated cells, (b) treated with the indicated IOH-NP concentration (1-50 µL/200 µL), and (c) treated with the freely dissolved drugs. The concentrations of the freely dissolved drugs were according to their dose in the IOH-NPs. Dotted red lines indicate the self-absorption of medium, cells, and/or drugs. Error bars correspond to standard error of $n = 4$.

Incucyte assays. AsPC1 and pH8N8 cells were plated, cultivated, and treated the same way as described for the aforementioned MTT assays and imaged over time with the Incucyte live-cell-analysis system (Sartorius, Germany). Imaging was started directly after adding the treatments and continued for 4 days. Images were recorded every hour using a standard 10× objective. The experiments were performed in triplicate. Two images per each well were recorded at defined positions. Representative images are shown in Figures S14-S21 for AsPC1 and pH8N8 cells at different drug concentrations (1-50 µL/200 µL) and over different time scales (0-72 h).

The cytotoxic efficacy of IOH-NPs with chemotherapeutic cocktail, first of all, was evaluated in *in vitro* studies with the single-drug $Gd^{3+}{}_2[PMX]^{2-}{}_3$ and $[Gd(OH)]^{2+}[EMP]^{2-}$ IOH-NPs using pH8N8 murine breast cancer cells and AsPC1 human pancreatic cancer cells. On the

one hand, these results were compared with dual-drug $Gd^{3+}_2[(PMX)_{0.5}(EMP)_{0.5}]^{2-}_3$ IOH-NPs (*see main paper: Figure 4*). On the other hand, the activity of the IOH-NPs was compared with the freely dissolved drugs PMX ($Na_2(PMX)\times 7H_2O$) (Figure S12), EMP ($Na_2(EMP)$) (Figure S13), as well as untreated cells (phosphate-buffered saline/PBS only) (Figures S12,S13; *see main paper: Figure 4*). The concentrations of the freely dissolved drugs were according to their dose in the IOH-NPs. Dotted red lines indicate the self-absorption of medium, drugs, and/or IOH-NPs, which needs to be taken into account to evaluate the cell growth.

In addition to the aforementioned cytotoxic efficacy (Figures S12,S13; *see main paper: Figure 4*), cell-based assays monitored by Incucyte were performed over 0-72 hours with AsPC1 and pH8N8 cells incubated with a concentration of NPs of 1-50 µL/200 µL medium (Figures S14-S21). All IOH-NPs show a clear time-dependent and concentration-dependent cytotoxic effect on the tumour cells. Even at low concentration (5 µL/200 µL) and short time of incubation (24 hours), the cell morphology is changing significantly. Detachment and swelling of cells, beginning deformation of nuclei, and accumulation of perinuclear vesicular structures indicate beginning cell death. This confirms the chemotherapeutic IOH-NPs not only to be effectively internalized by the cells but to also evidently release their drug load, resulting in the expected concentration-dependent cytotoxic efficacy. Similar to the results of the MTT-based viability test, pH8N8 cells are more affected by EMP (Figures S18-S21), whereas PMX shows a higher activity on AsPC1 cells (Figures S14-S17). Beside cell remains, an increasing number of IOH-NP agglomerates is visible, especially at high IOH-NP concentrations (10 and 50 µL/200 µL). At high IOH-NP concentrations, thus, IOH-NPs are still present without having released their full drug load although all cells are dead. Beside this qualitative evaluation, a quantification of cell density reflecting cell growth is difficult since the remains of dead cells and IOH-NP agglomerates are difficult to differentiate (Figures S14-S21).

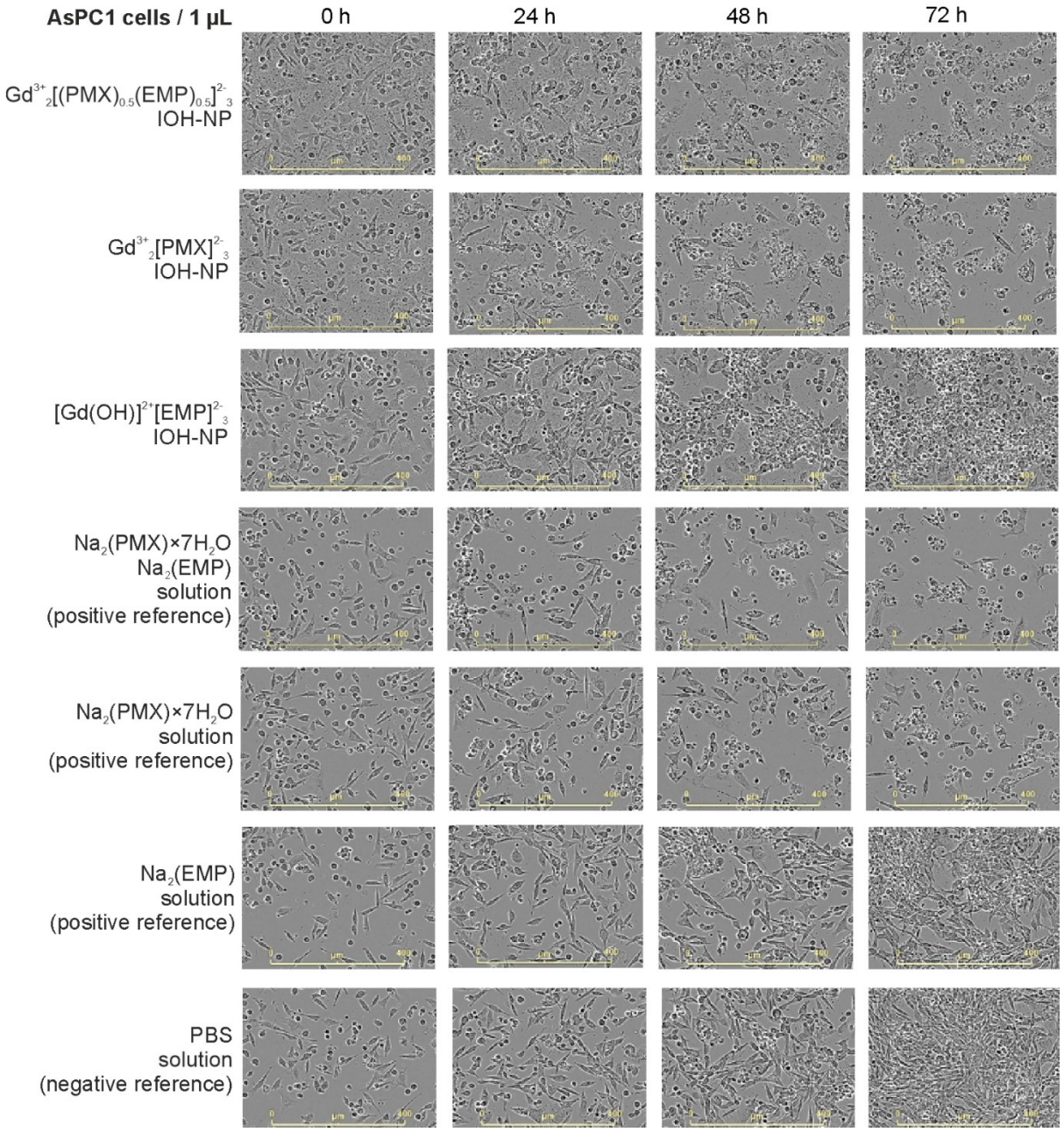

Figure S14. Representative images obtained with the Incucyte system applying AsPC1 cells incubated with a concentration of 1 µL/200 µL of different IOH-NPs over 0-72 hours (yellow scale bar: 400 µm).

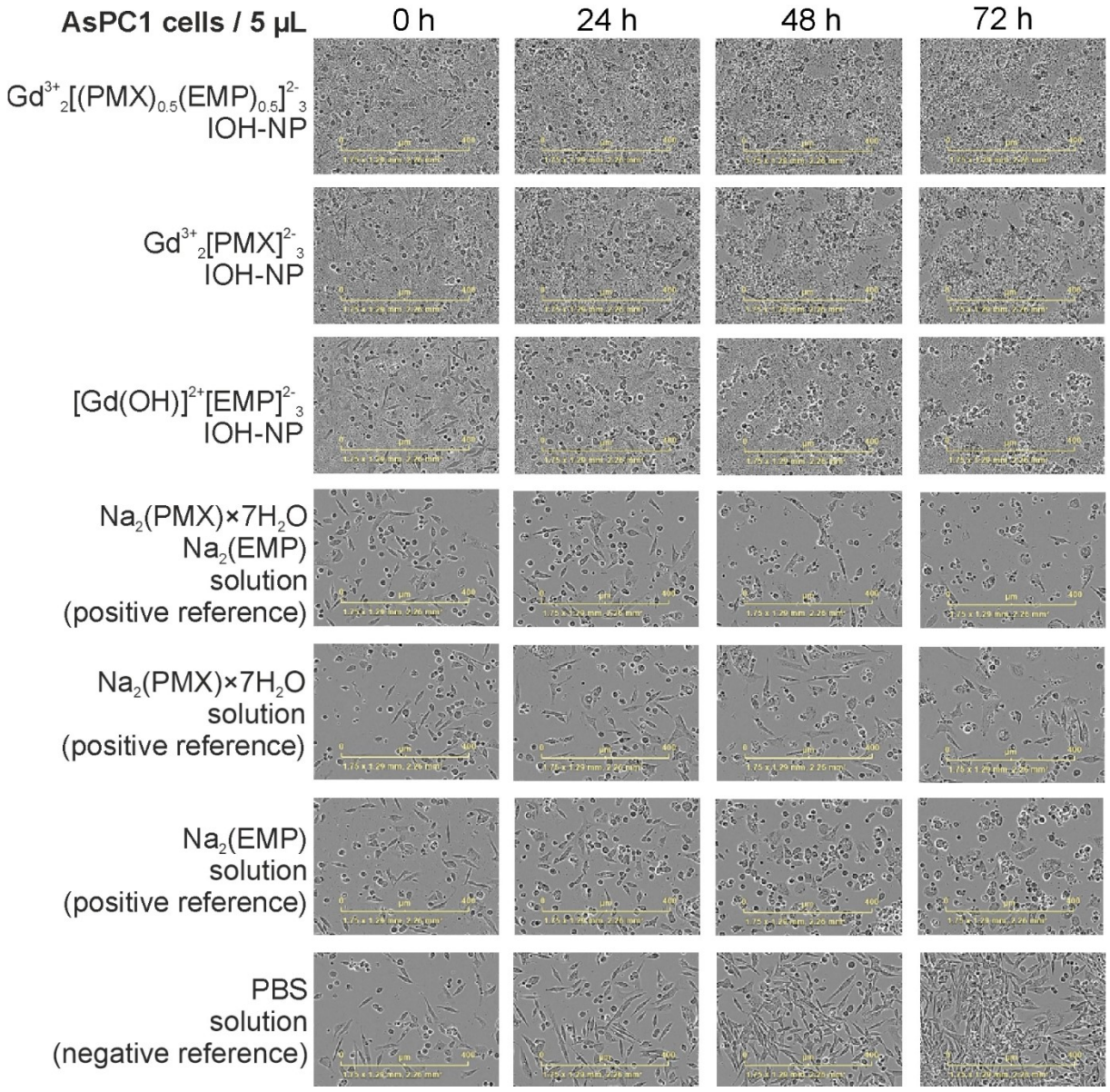

Figure S15. Representative images obtained with the Incucyte system applying AsPC1 cells incubated with a concentration of 5 µL/200 µL of different IOH-NPs over 0-72 hours (yellow scale bar: 400 µm).

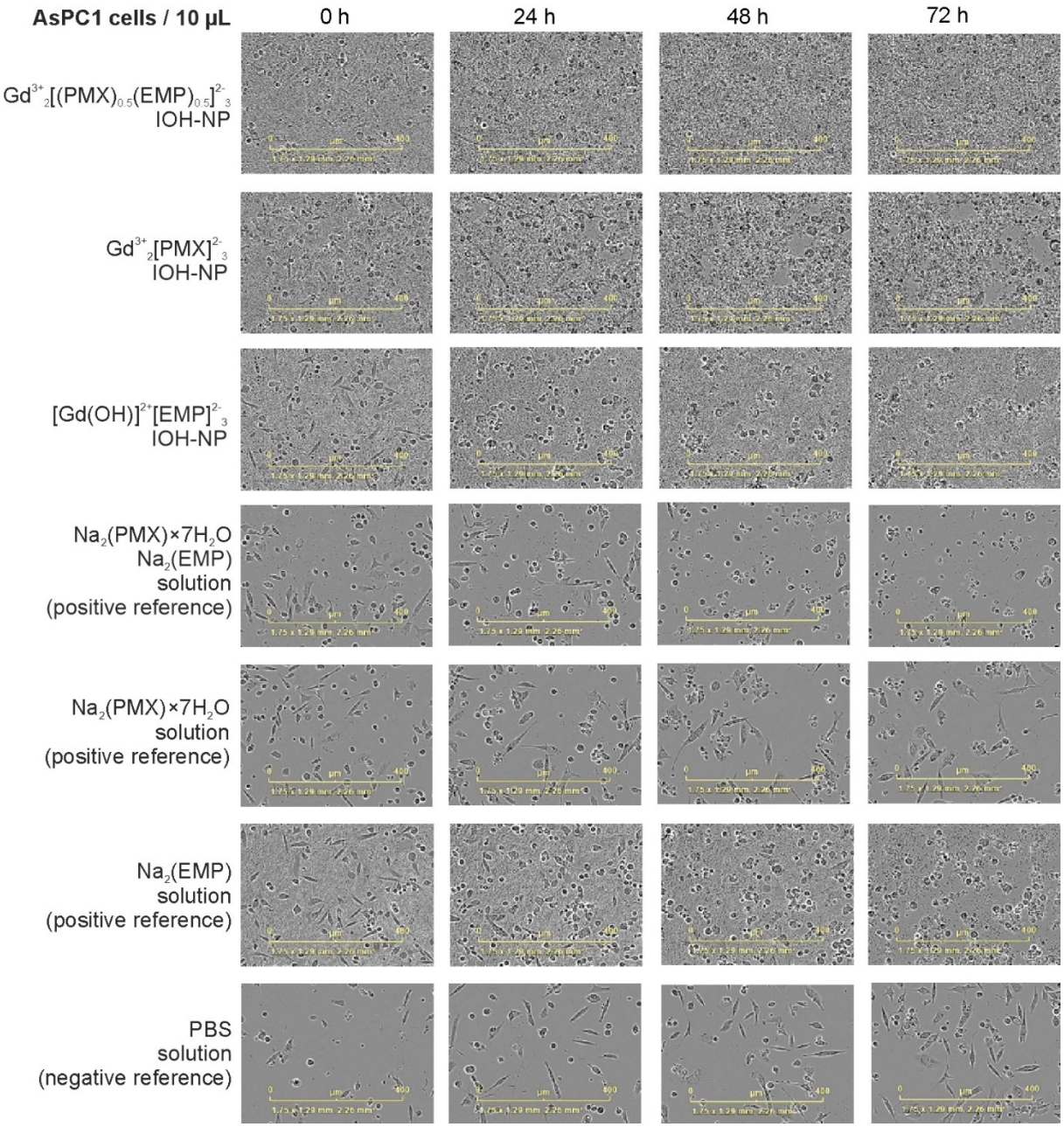

Figure S16. Representative images obtained with the Incucyte system applying AsPC1 cells incubated with a concentration of 10 µL/200 µL of different IOH-NPs over 0-72 hours (yellow scale bar: 400 µm).

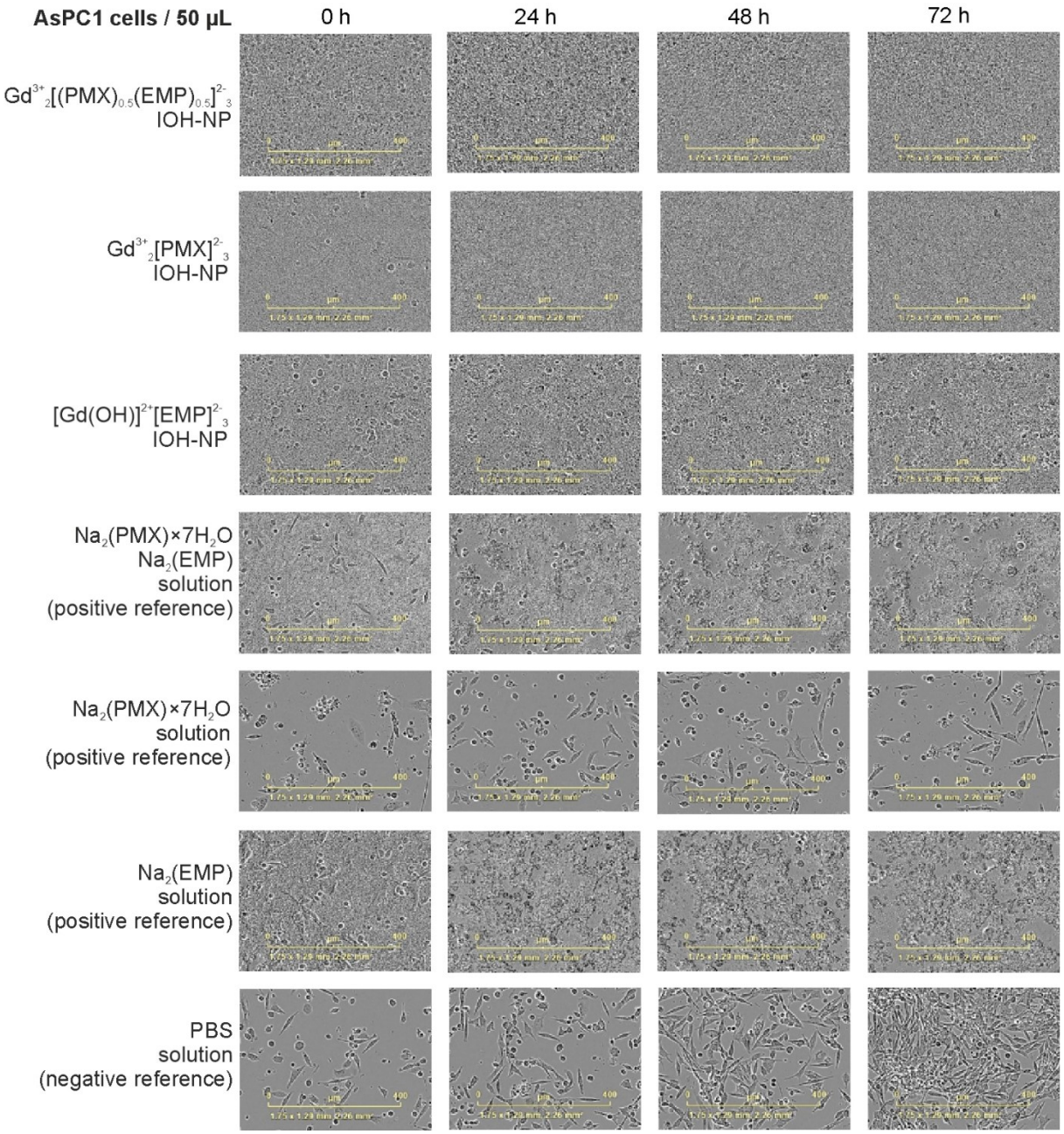

Figure S17. Representative images obtained with the Incucyte system applying AsPC1 cells incubated with a concentration of 50 µL/200 µL of different IOH-NPs over 0-72 hours (yellow scale bar: 400 µm).

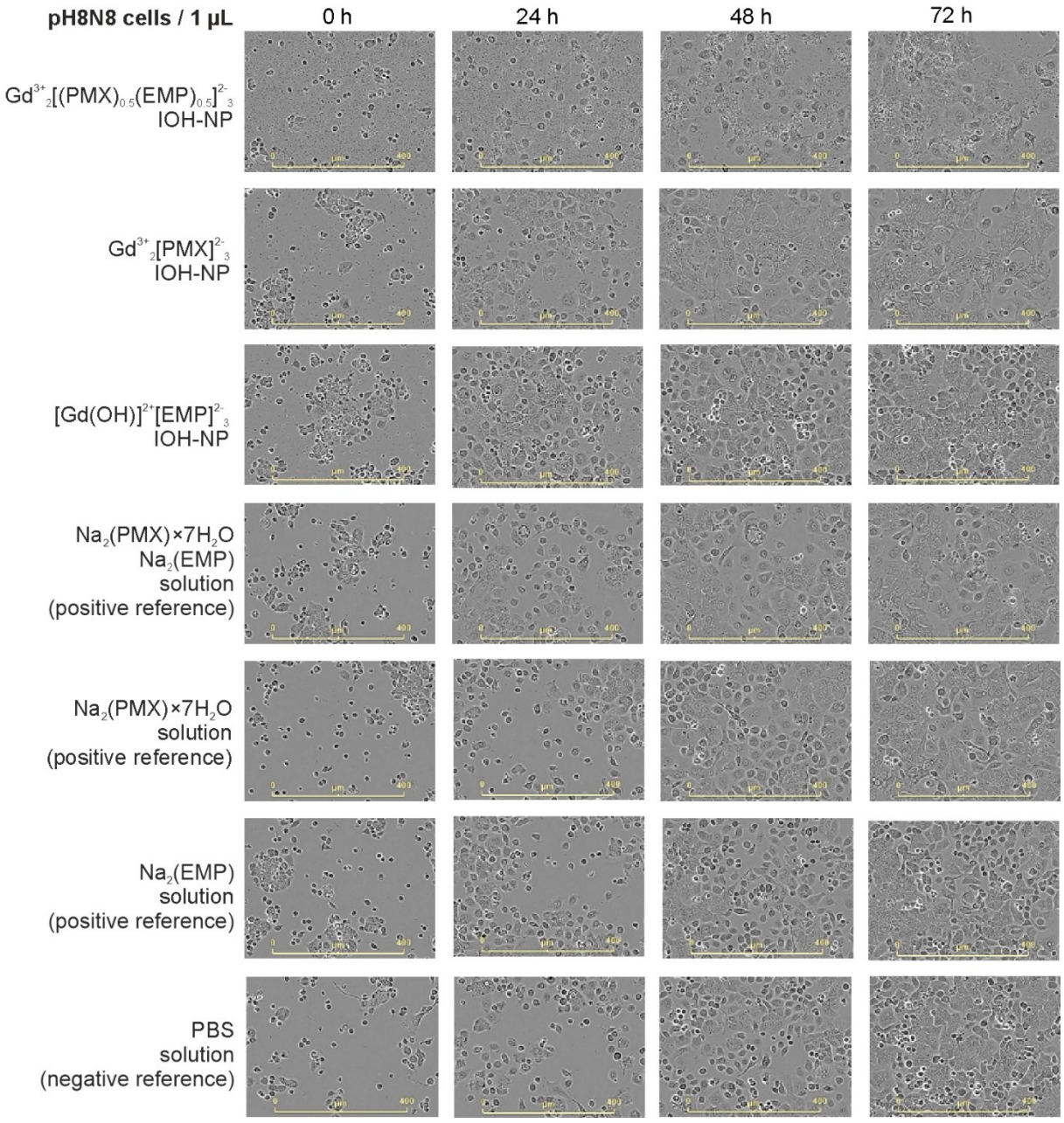

Figure S18. Representative images obtained with the Incucyte system applying pH8N8 cells incubated with a concentration of 1 µL/200 µL of different IOH-NPs over 0-72 hours (yellow scale bar: 400 µm).

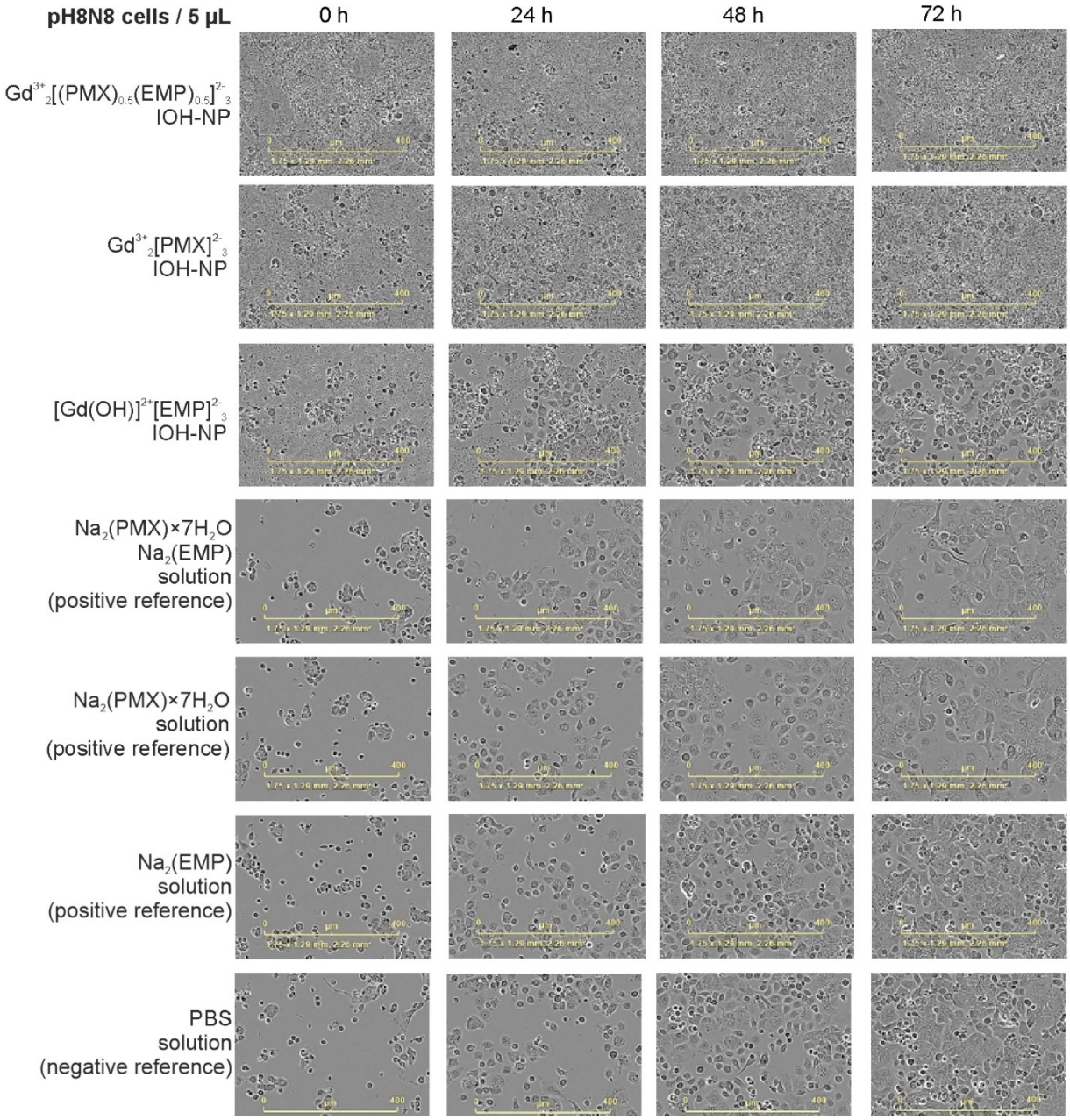

Figure S19. Representative images obtained with the Incucyte system applying pH8N8 cells incubated with a concentration of 5 µL/200 µL of different IOH-NPs over 0-72 hours (yellow scale bar: 400 µm).

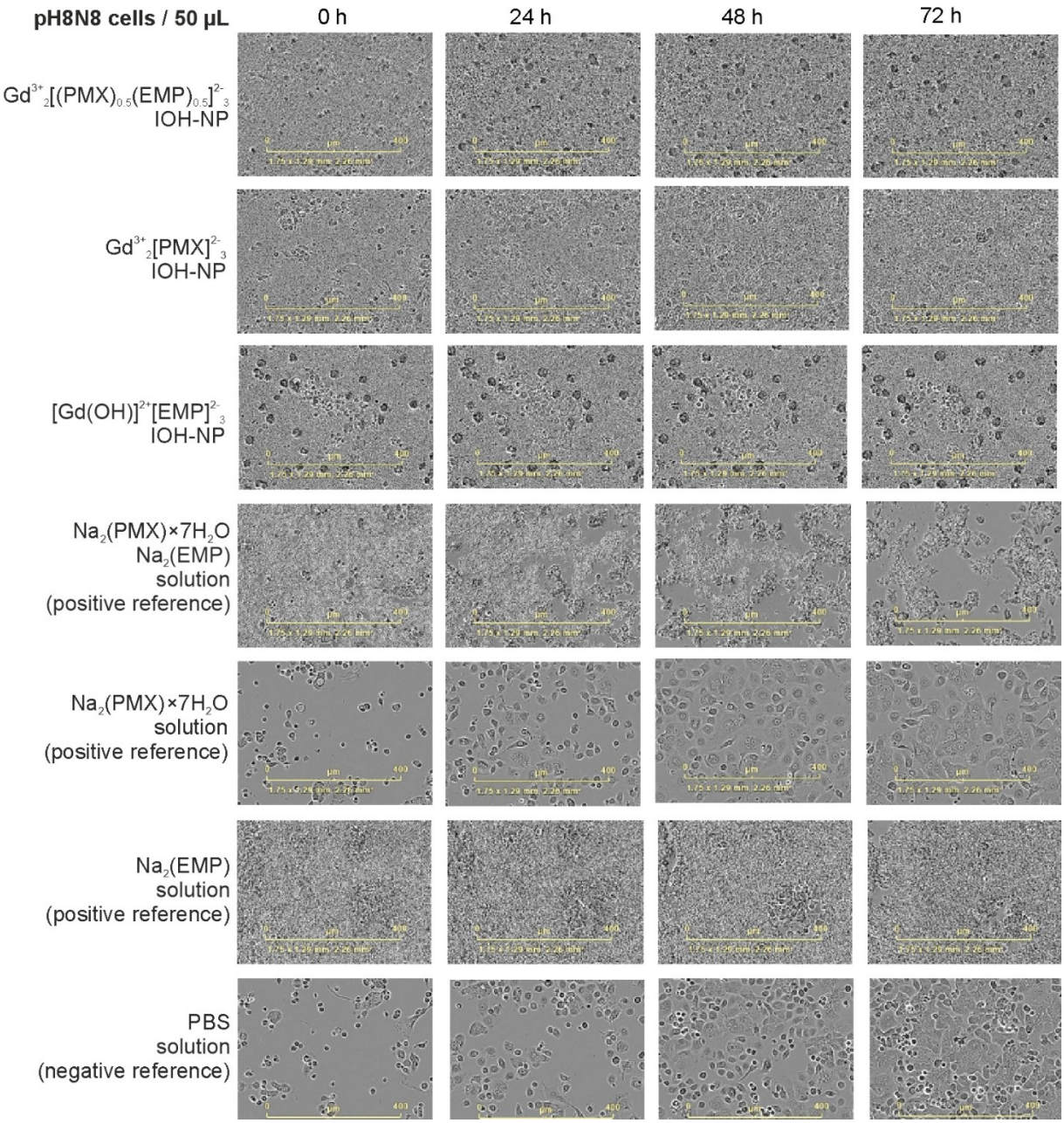

Figure S20. Representative images obtained with the Incucyte system applying pH8N8 cells incubated with a concentration of 10 µL/200 µL of different IOH-NPs over 0-72 hours (yellow scale bar: 400 µm).

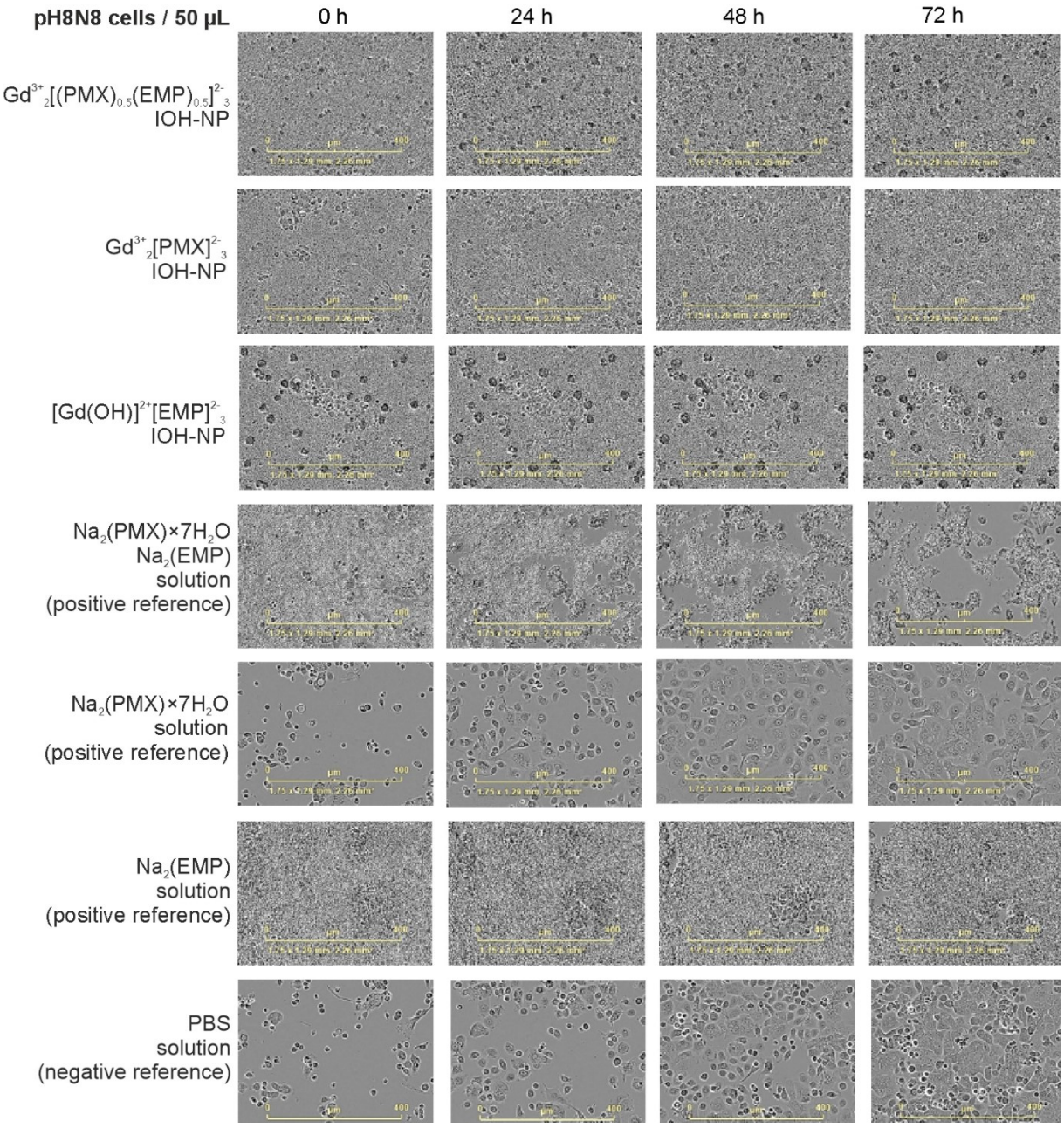

Figure S21. Representative images obtained with the Incucyte system applying pH8N8 cells incubated with a concentration of 50 µL/200 µL of different IOH-NPs over 0-72 hours (yellow scale bar: 400 µm).

5. Material Characterization of IOH-NPs with Phototoxic Agents

Prior to *in vitro* studies for IOH-NPs with cytotoxic and phototoxic agents, the formation of reactive oxygen species (ROS) was proven with single-agent $Gd_4^{3+}[AlPCS_4]_3^{4-}$ and $La_4^{3+}[TPPS_4]_3^{4-}$ IOH-NPs. These studies were performed and published before.[S4] Therefore, only the essential aspects are summarized here as far as they are relevant for the novel dual-function IOH-NPs, which we report for the first time.

For both IOH-NPs, ROS formation as well as the quantum yield (φ_Δ) for singlet oxygen production were evaluated using different methods. For $Gd_4^{3+}[AlPCS_4]_3^{4-}$, φ_Δ was determined by a relative method using DPBF (1,3-diphenylisobenzofuran) as a chemical quencher for $^1O_2$ oxygen.[S4,S5] Accordingly, φ_Δ is proportional to the decrease of the DBPF absorption band under illumination and can be recorded via UV-Vis spectroscopy along with the irradiation time (Figure S22a). In difference, φ_Δ for $La_4^{3+}[TPPS_4]_3^{4-}$ IOH-NPs was determined by the iodide method based on the reaction of $^1O_2$ with I^- in the presence of $(NH_4)_2MoO_4$ as a catalyst.[S4,S5] As a result, I_3^- is produced in an amount directly proportional to the generated $^1O_2$. Here, the increase of the absorption band of I_3^- can be monitored spectroscopically along with radiation time (Figure S22b). It needs to be noticed that the more common DPBF method cannot be used in the case of $La_4^{3+}[TPPS_4]_3^{4-}$ since its absorption overlays the DPBF band.[S4,S5]

Based on the above described methods, the quantum yield for $^1O_2$ production was determined to 37% for $Gd_4^{3+}[AlPCS_4]_3^{4-}$ and 49% for $La_4^{3+}[TPPS_4]_3^{4-}$.[S4] These values are similar to freely dissolved $H_4(AlPCS_4)$ (34%) and $H_4(TPPS_4)$ (51%) in aqueous solution.[S5]

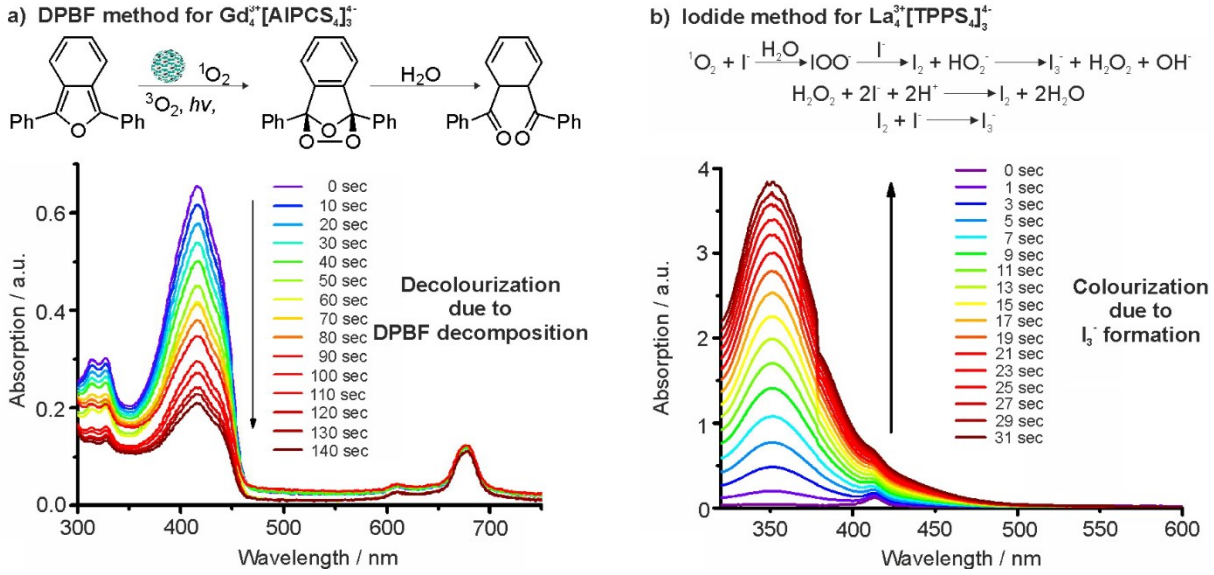

Figure S22. Spectroscopic prove and determination of ROS formation and quantum yield (φ_Δ) for $^1O_2$ production of the photoactive IOH-NPs: (a) DPBF method for $Gd_4^{3+}[AlPCS_4]_3^{4-}$;[S4,S5] (b) Iodide method for $La_4^{3+}[TPPS_4]_3^{4-}$.[S4,S5]

6. *In vitro* Studies for IOH-NPs with Cytotoxic and Phototoxic Agents

Cell culture. Cells were cultured in DMEM (HCT116, NHDF, HeLa-GFP, HepG2 cells) with 1% penicillin/streptomycin (Thermo Fischer Scientific, Germany) and 10% FCS (Thermo

Fischer Scientific, Germany) or EGM-2 medium (HUVEC with EGM-2 additives (Lonza, Germany) with standard cell culture conditions (37 °C, humidified atmosphere with 5% CO_2).

Incubation with IOH-NPs. The cells (HeLa-GFP) were seeded on 8-well μ-slides (2×10^4 cells per well) in DMEM and incubated at 37 °C (5% CO_2) for 24 h. The medium was replaced by fresh medium with different concentrations of the IOH-NPs as indicated in the experiments. The cells were incubated for 24 h. Before the experiments, the cells were washed with DPBS (Thermo Fischer Scientific, Germany) and new cell medium was added.

Confocal microscopy on HeLa-GFP and HUVEC-GFP cells pre-treated with IOH-NPs was conducted using a TCS SPE DMI4000B inverted microscope (Leica Microsystems, Germany) (Figure S23). Sample illumination for PDT studies was performed for 20 min at 635 nm ($AlPCS_4$) or 532 nm ($TPPS_4$). The images were taken at excitation/emission: 488 nm/500-540 nm (GFP), 532 nm/ 50-650 nm ($TPPS_4$), and 635 nm/650-750 nm ($AlPCS_4$).

Cell viability assay (MTT assay): 1×10^4 HCT116 and NHDF cells per well were cultured in in 96-well plates in DMEM supplemented with 1% penicillin/streptomycin and 10% FCS and incubated (37 °C, 5% CO_2) for 24 h (HUVEC in EGM-2 medium with EGM-2 additives). Then, the medium was removed, and the IOH-NPs as well as the dissolved photosensitizers and drugs in the culture medium were added. For negative controls of the experiment, only the medium was exchanged. The illumination and activation of the photosensitizers was performed 24 h after the treatment in case of $AlPCS_4$ using a Pearl® Imager (LI-COR® Biosciences, Germany) at 700 nm for 30 min. $TPPS_4$ samples were exposed for 3 min to white light emitted by an Ultra Vitralux 300W E27 lamp (OSRAM, Germany). After 72 h, the cells were subjected to an MTT assay (Promega, Germany). Thus, 15 µL of MTT dye solution were added into each well. After 3 h, the cells were lysed by addition of the MTT stop solution (100 µL per well, Promega, Germany) and incubated overnight. The positive controls were treated with 1% Triton-X-100 (Serva Electrophoresis, Germany) before subjected to the MTT assay (Figures S24,S25). The cell viability as a test over control [TO] was determined by measuring the absorbance of the formazan dye at 595 nm by using the SpectraMax® Microplate Reader (Molecular Devices LLC, Germany).

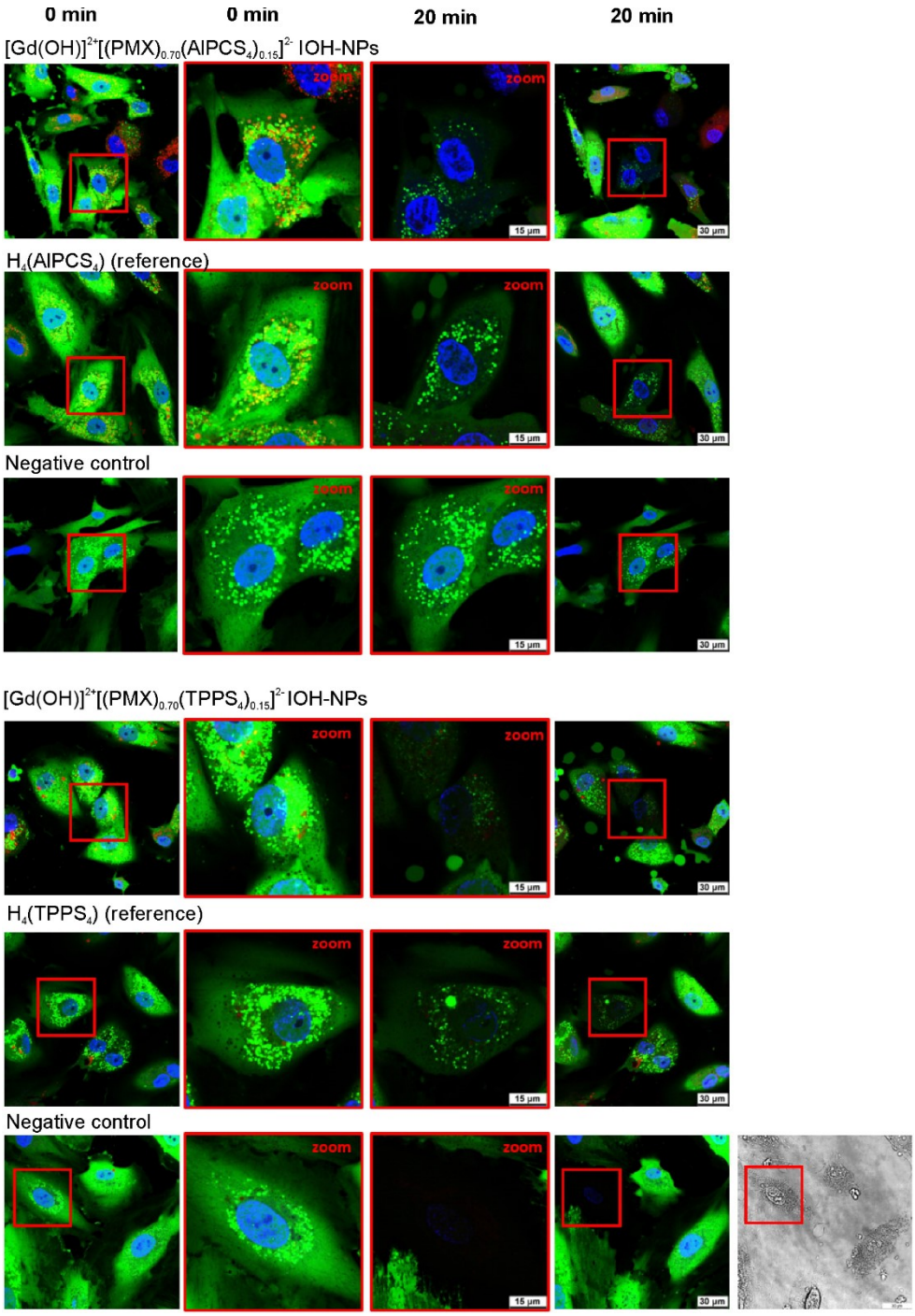

Figure S23. Confocal microscopy images of HUVEC-GFP cells after incubation with $[Gd(OH)]^{2+}[(PMX)_{0.74}(AlPCS_4)_{0.13}]^{2-}$ and $[Gd(OH)]^{2+}[(PMX)_{0.70}(TPPS_4)_{0.15}]^{2-}$ IOH-NPs (50 µg/mL) as well as with the freely dissolved photoactive agents $AlPCS_4$ (15.5 µg/mL) and $TPPS_4$ (16.0 µg/mL) for 24 h. Cells were illuminated in the marked area (red square) for 20 min at 635 nm ($AlPCS_4$) or 532 nm ($TPPS_4$). Untreated HeLa-GFP cells ±illumination were used as negative control. Hoechst 33342 (2 µg/mL) was used for nuclear stain (λ_{exc} = 405 nm, λ_{em} = 410-450 nm). Depicted are the merged images of the fluorescence emission for GFP (λ_{exc} = 488 nm, λ_{em} = 500-540 nm), Hoechst and the IOH-NPs (λ_{exc} = 635 nm, λ_{em} = 650-750 nm for $AlPCS_4$; λ_{exc} = 532 nm, λ_{em} = 550-650 nm for $TPPS_4$).

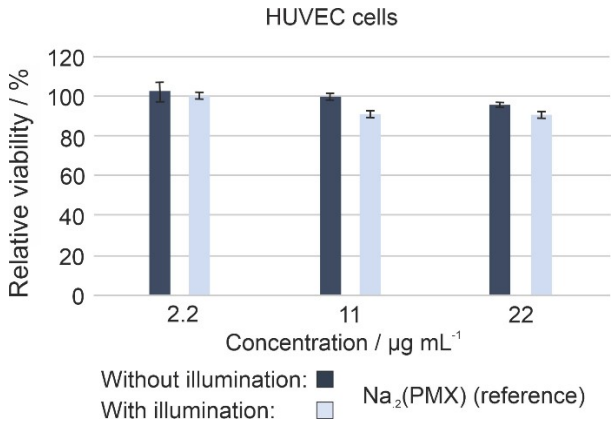

Figure S24. Cell viability assays for PMX on human umbilical vein endothelial cells (HUVEC) ±illumination. HUVEC cells were treated with different concentrations of PMX (2.2, 11, 22 µg/mL) (corresponding to the PMX concentration in the 5, 25, 50 µg/mL IOH-NPs). 24 h after treatment, the samples were exposed to an illumination at 700 nm for 30 min.

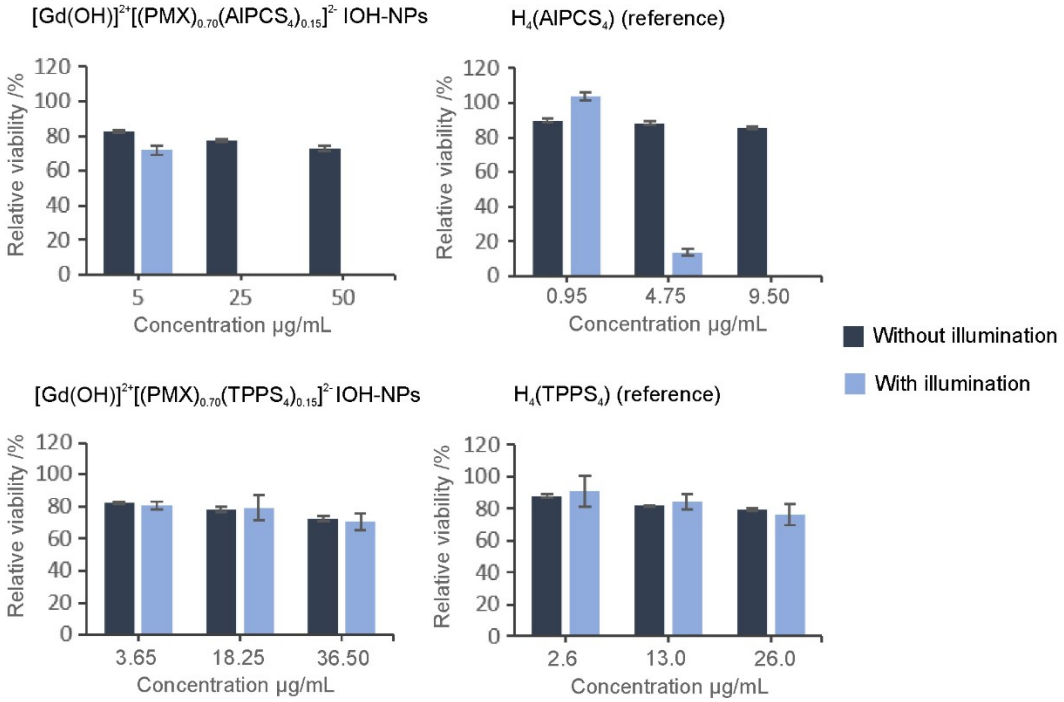

Figure S25. Cell viability assay with human-skin-carcinoma cells (SK-Mel-28) of $[Gd(OH)]^{2+}[(PMX)_{0.74}(AlPCS_4)_{0.13}]^{2-}$ (5, 25, 50 µg/mL), $Gd^{3+}{}_2[PMX]^{2-}{}_3$ (3.65, 18.25, 36.5 µg/mL) and the freely dissolved active agents $AlPCS_4$ (0.95, 4.75, 9.5 µg/mL) and PMX (2.6, 13, 26 µg/mL) for 48 h. The concentrations of the freely dissolved agents were according to their dose in the IOH-NPs. Eventually, the cells were illuminated for 30 min at 700 nm after 24 h and further incubated for a total of 48 h. The experiments were performed in triplicates. Values are expressed as the mean ±SD (n = 3).

Angiogenesis. To determine the impact of the IOH-NPs on the formation of new microcapillaries from endothelial cells, 8-well μ-slides were coated with 60 µL Geltrex® solution (Thermo Fischer Scientific, Germany) per well and incubated overnight. 4×10^4 HUVEC in 160 µL EGM-2 medium were seeded in each well. The IOH-NPs and the freely dissolved photosensitizers were added. After 1 h as well as after 3 h, illuminations with 700 nm light for $AlPCS_4$ (40 min) and white light for $TPPS_4$ (3 min) were performed, respectively, followed by further incubation of 24 h. Thereafter, the cell samples were stained with Hoechst 33342 (2.0 mg/mL) and examined via confocal microscopy (TCS SPE DMI4000B inverted microscope, Leica Microsystems, Germany). The images were taken at excitation/emission: 405 nm/410-450 nm for Hoechst 33342.

3D cell culture. Spheroids were used for drug efficacy testing for the detection of cytotoxic, phototoxic and anti-proliferative effects in 3D cell culture (Figures S26,S27; *see main paper: Figure 11*). Cells were seeded at a concentration of 3000 cells per well in agarose-treated 96-well plates, and cultured for 3 days before being treated with the IOH-NPs or the freely dissolved agents. One day after treatment, the cells were eventually illuminated for 30 min at 700 nm (for $AlPCS_4$) or white light (for $TPPS_4$) and further incubated. Toxicity assays were performed as previously described. To examine the spheroid growth over time, spheroids were imaged 7 days using light microscopy. The spheroid diameter was measured by LAS X Leica Software. Values are expressed as the mean ±SD (n = 6).

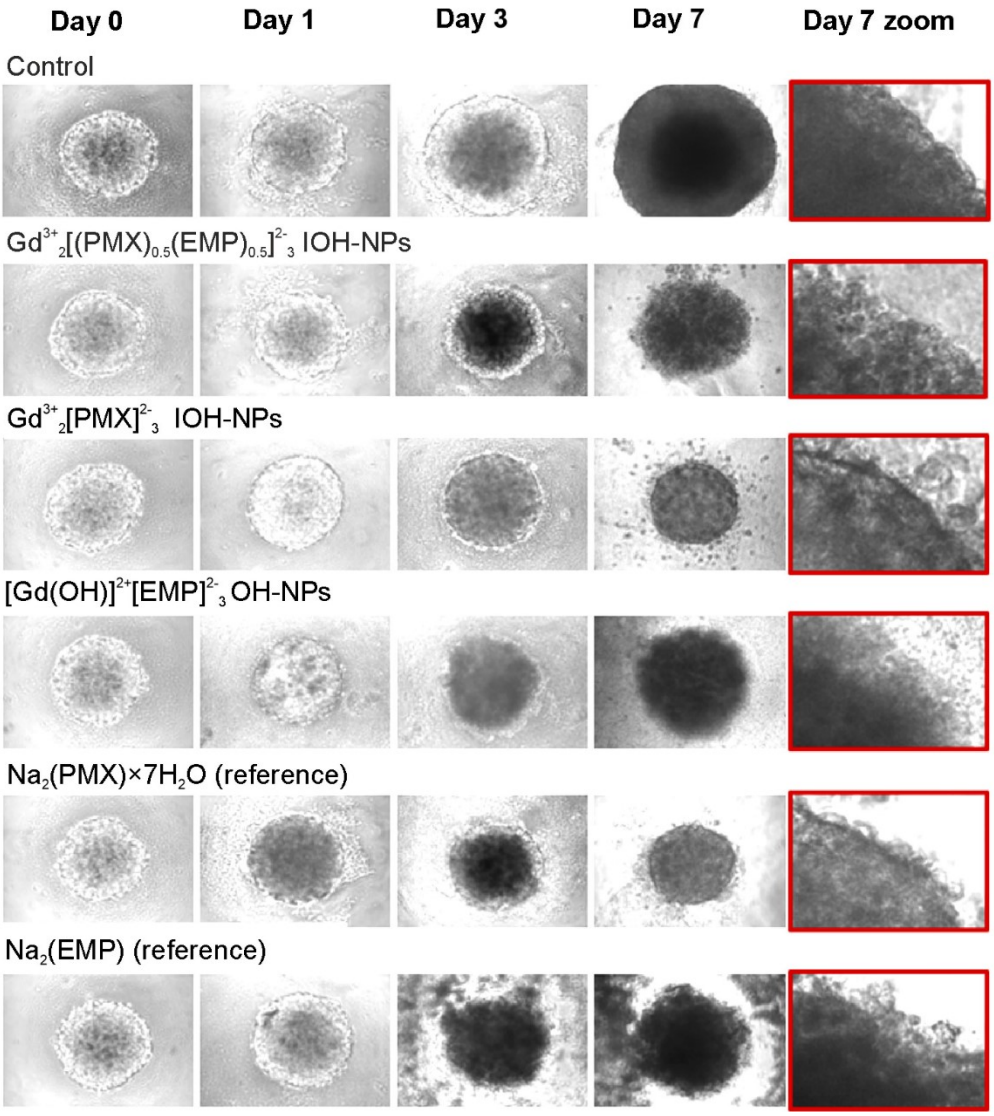

Figure S26. Measurement of HepG2 spheroid growth before treatment and 1, 3, 7 days after treatment. Spheroids were treated with 100 µg/mL of $Gd^{3+}_2[(PMX)_{0.5}(EMP)_{0.5}]^{2-}_3$, $Gd^{3+}_2[PMX]^{2-}_3$ and $[Gd(OH)]^{2+}[EMP]^{2-}$ IOH-NPs as well as the freely dissolved reference drugs $Na_2(PMX)\times 7H_2O$ and $Na_2(EMP)$ (112.5 µg/mL PMX, 79.0 µg/mL EMP). The concentrations of the freely dissolved drugs are identical to their dose in the IOH-NPs. The control shows the morphological change of spheroids during the 7-day treatment. The samples show the size change of HepG2 tumour spheroids compared to the control group during the 7-day treatment. Values are expressed as the mean ±SD (n = 6).

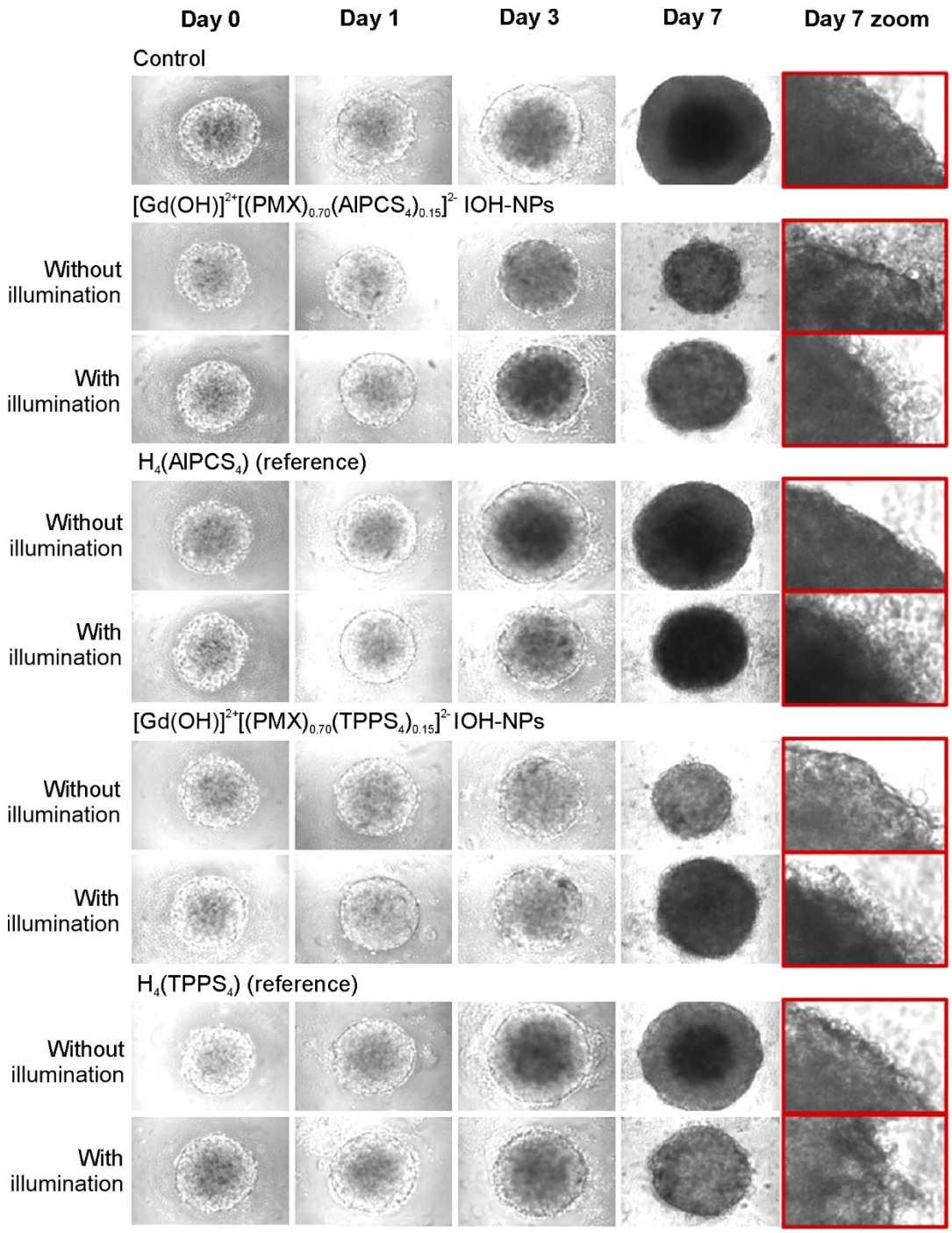

Figure S27. Measurement of HepG2 spheroid growth before treatment and 1, 3, 7 days after treatment. Spheroids were treated with 100 µg/mL of $[Gd(OH)]^{2+}[(PMX)_{0.74}(AlPCS_4)_{0.13}]^{2-}$ and $[Gd(OH)]^{2+}[(PMX)_{0.70}(TPPS_4)_{0.15}]^{2-}$ IOH-NPs as well as the freely dissolved photoactive agents $H_4(AlPCS_4)$ and $H_4(TPPS_4)$ (31 µg/mL $AlPCS_4$, 32 µg/mL $TPPS_4$). The concentrations of the freely dissolved photoactive agents are identical to their dose in the IOH-NPs. The control shows the morphological change of spheroids during the 7-day treatment. The samples show the size change of HepG2 tumour spheroids compared to the control group during the 7-day treatment. Values are expressed as the mean ±SD (n = 6).

References

S1 (a) W. Pawlina and M. A. Ross, *Histology: A Text and Atlas.* 8th Ed., Walters Kluwer, Philadelphia **2020**. (b) Z. Starosolski, R. Bhavane, K. B. Ghaghada, S. A. Vasudevan, A. Kaay and A. Annapragada, *PLoS One,* 2017, **12**, e0187563.

S2 C. Maenz, E. Lenfert, K. Pantel, U. Schumacher, W. Deppert and F. Wegwitz, *BMC Cancer*, 2015, **15**, 178.

S3 J. Schindelin, I. Arganda-Carreras, E. Frise, V. Kaynig, M. Longair, T. Pietzsch, S. Preibisch, C. Rueden, S. Saalfeld, B. Schmid, J.-Y. Tinevez, D. J. White, V. Hartenstein, K. Eliceiri, P. Tomancak and A. Cardona, *Nature Meth.*, 2012, **9**, 676-682.

S4 (a) M. Poß, H. Gröger and C. Feldmann, *Chem. Commun.,* 2018, **54**, 1245-1248. (b) B. L. Neumeier, M. Khorenko, F. Alves, O. Goldmann, J. Napp, U. Schepers, H. M. Reichardt and C. Feldmann, *ChemNanoMat,* 2018, **4**, 1-23.

S5 (a) J. Mosinger and Z. Mi̇čka, *J. Photochem. Photobiol. A,* 1997, **107**, 77. (b) W. P. Helman and A. B. Ross, *J. Phys. Chem.,* **1993,** 22*,* 113.